Synthesis and Characterization of Chemically Etched Nanostructured Silicon

Thesis by

Asad Jahangir Mughal

In Partial Fulfillment of the Requirements

For the Degree of

Master of Science

King Abdullah University of Science and Technology

Thuwal, Kingdom of Saudi Arabia

May 2012

EXAMINATION COMMITTEE APPROVALS FORM

The dissertation/thesis of Asad Jahangir Mughal is approved by the examination committee.

Committee Chairperson Dr. Saharoui Chaieb

Committee Member Dr. Osman Bakr

Committee Member Dr. Boon Ooi

ABSTRACT

Synthesis and Characterization of Chemically Etched Nanostructured Silicon

Asad Jahangir Mughal

Silicon is an essential element in today's modern world. Nanostructured Si is a more recently studied variant, which has currently garnered much attention. When its spatial dimensions are confined below a certain limit, its optical properties change dramatically. It transforms from an indirect bandgap material that does not absorb or emit light efficiently into one which can emit visible light at room temperatures. Although much work has been conducted in understanding the properties of nanostructured Si, in particular porous Si surfaces, a clear understanding of the origin of photoluminescence has not yet been produced. Typical synthesis approaches used to produce nanostructured Si, in particular porous Si and nanocrystalline Si have involved complex preparations used at high temperatures, pressures, or currents. The purpose of this thesis is to develop an easier synthesis approach to produce nanostructured Si as well as arrive at a clearer understanding of the origin of photoluminescence in these systems.

We used a simple chemical etching technique followed by sonication to produce nanostructured Si suspensions. The etching process involved producing pores on the surface of a Si substrate in a solution containing hydrofluoric acid and an oxidant. Nanocrystalline Si as well as nanoscale amorphous porous Si suspensions were successfully synthesized using this process. We probed into the phase,

composition, and origin of photoluminescence in these materials, through the use of several characterization techniques. TEM and SEM were used to determine morphology and phase. FT-IR and XPS were employed to study chemical compositions, and steady state and time resolved optical spectroscopy techniques were applied to resolve their photoluminescent properties.

Our work has revealed that the type of oxidant utilized during etching had a significant impact on the final product. When using nitric acid as the oxidant, we formed nanocrystalline Si suspensions composed of particles with a crystal structure different than the common polymorph of Si. These particles emitted UV to blue wavelengths. Iron(III) chloride was also employed as an oxidant, and it created amorphous Si nanostructures from a bulk crystalline Si source. These suspensions showed ultra-bright visible photoluminescence, which could be tuned through engineering the surface.

ACKNOWLEDGEMENTS

I would like to thank my committee chair/thesis advisor, Dr. Sahraoui Chaieb, for his guidance and support throughout the course of this research. His insights on conducting independent scientific research were invaluable and greatly appreciated. I also thank Dr. Osman Bakr for the fruitful discussions we have had. The friendship and support I have received from all the members of Dr. Chaieb's group during my time at KAUST is also greatly cherished.

Characterization is an essential element in materials science research. On that note, I would like to recognize all the KAUST Core Lab staff members that have assisted me in my work. I would especially like to thank Dr. Dalaver Anjum and Dr. Rachit Sougrat for their support in TEM analysis.

My appreciation also goes to my friends, colleagues, and the department faculty and staff for making my time at King Abdullah University of Science and Technology a memorable experience.

Finally, my heartfelt gratitude is extended to my family for their encouragement and to my wife, Mehreen, for her patience and support.

TABLE OF CONTENTS

Page

LIST OF ABBREVIATIONS

ap-Si	Amorphous porous silicon
a-Si	Amorphous silicon
at. %	Atomic percent
EDS	Energy dispersive spectroscopy
EDS	Energy dispersive spectroscopy
FFT	Fast Fourier Transform
FT-IR	Fourier transformed infrared spectroscopy
IPA	Isopropyl alcohol
IR	Infrared
LED	Light emitting diode
MeCN	Acetonitrile
nc-Si	Nanocrystalline silicon
PECVD	Plasma enhanced chemical vapor deposition
PL	Photoluminescence
p-Si	Porous silicon
SAED	Selected area electron diffraction
SEM	Scanning electron microscopy
STEM	Scanning transmission electron microscopy
TEM	Transmission electron microscopy
TEM	Transmission electron microscopy
THF	Tetrahydrofuran
TA	Transvers acoustic phonon mode
TO	Transvers optical phonon mode
UV	Ultraviolet
XPS	x-ray photoelectron spectroscopy

LIST OF SYMBOLS

$E_{binding}$	Electron binding energy
E_o	Standard electrode potential
E_{photon}	Energy of the incoming X-ray
k	crystal momentum
P	Intensity of transmitted light
P_0	Intensity of the monochromatic light
R_0	Localization radius
R_c	Non-radiative capture radius
t	Time
V_c	Non-radiative capture volume
v_m	Monolayer of adsorbed gas
$\Delta\theta$	Root mean square, rms, bond angle disorder
τ	Radiative lifetime
Φ	Work function of the XPS spectrometer
ω_0	Attempt to escape frequency

LIST OF ILLUSTRATIONS

LIST OF TABLES

1 INTRODUCTION

1.1 Nanostructured Si

Silicon is the second most abundant element on the surface of the earth [1]. It is also the most widely used semiconductor in electronics and photovoltaic applications. Given its abundance and importance in our daily lives, a great deal of research has gone into this material for its use in a wide array of industrial applications. Understanding its physical properties is crucial for its use in real world applications.

Bulk crystalline Si, a common form of Silicon, does not exhibit efficient light emission at room temperature, making it a poor active material in optoelectronic devices. This is mainly due to its band structure having an indirect band gap of 1.1 eV. An indirect band gap requires optical transitions between energy bands to emit phonons, in addition to photons, in order to conserve crystal momentum. However, with the proper structure Si can overcome its very low intrinsic radiative recombination probability and be made to become an efficient emitter of light at room temperature. One method to overcoming the indirect nature of optical transition in Si is through the relaxation of momentum (k) selection rule caused by spatially confining it into low dimensional nanostructures. This discovery of visible luminescence makes it possible for Si to be used in optoelectronic applications.

Nanostructured Si is a wide field of research. In this work, we will focus on synthesizing and characterizing the properties of Si structures derived from porous Si films created through a chemical etching process. The mechanism behind the emission of visible light from these materials will be discussed as well.

1.2 Objectives of the Research

The three major objectives of this research are listed below:

1. Synthesize and characterize free standing nanocrystalline Si (nc-Si) produced through a stain etching method using nitric acid
2. Synthesis and characterize amorphous porous Si (ap-Si) suspensions produced through a stain etching method using iron(III) chloride
3. Study the effect of surface states on the emission from ap-Si

1.3 Organization of this Thesis

This thesis is organized into six chapters. The next chapter provides a review of work done in this field of study, with a focus on synthesis methods and the mechanism for the emission of light. An explanation of the methods and materials used during the course of the research are provided in chapter three. Chapter four reports and discusses the results of chemical etching using nitric acid. The use of iron chloride in the synthesis of amorphous porous silicon is reported and discussed in chapter five. Finally, concluding remarks and recommendations for future work are presented in chapter six.

2 LITERATURE REVIEW

2.1 Introduction

Transforming bulk Si into nanometer scales results in changes to its electronic structure that allow it to become an efficient room temperature emitter of visible light. This unique property enables Si to become an optically active material which could be used in various applications.

For instance the optical properties of porous Silicon (p-Si) allow it to be implemented in a wide array of technologies such as optoelectronics[2], sensors[3], and photonic barcodes[4]. Its high surface area porous structure have even been shown to be applicable as cell cultures[5] , drug delivery systems[6], biomaterials[7], catalyzers for hydrogen production[8], solar cells, LEDs[9], and anodes for Li ion battery [10].

Nanocrystalline silicon (nc-Si) has also demonstrated its use in several applications. Since this material is biologically benign compared to other semiconductor nanocrystals(i.e. CdTe, PbS, etc.) [11], they have been shown to be good candidates for tagging biological material[12] and hybrid biofuel cells[13]. Their optoelectronic properties have allowed it to be used in devices such as LEDs[14], hybrid solar cells[15], super capacitors[16], biological sensors[17], and lasers[18]. They are even believed to be a component of interstellar dust[19].

In this chapter we will discuss the synthesis techniques currently employed in creating porous Si and nanocrystalline Si. We will then discuss the current understanding of the processes behind the emission of light in these materials.

2.2 Nanostructured Si

2.2.1 Porous Si

Porous silicon is an extensively studied variant of nano-scaled Si. The porous features in this material are typically created from a bulk Si surface through some form of electrochemical etching. The first reported observation of visible light-emission from anodically etched p-Si layers at room temperature was made by Canham more than two decades ago[20]. Since then a great deal of work has been published on its formation[21] , surface chemistry[22], structure, and photoluminescence[23].

2.2.2 Nanocrystalline Si

nc-Si are a class of nanostructured Si that has garnered a great deal of interest for the past decade. nc-Si are defined as particles of Si with a diameter less than its Bohr exciton radius of 5 nm. For semiconductors at these length scales quantum confinement effects dominate, allowing for tunable optical properties based on size[24].

Free standing nc-Si has been the focus of a great deal of research due to their unique chemical and optical properties. One of their advantages is the ability to alter their

surface chemistry which in turn can affect its optical properties and allow it to be further formed into hierarchical structures[25].

2.3 Synthesis of Nanostructured Si

2.3.1 Porous Si

There are various methods for creating p-Si layers on a Si substrate. The most common of which is known as anodic etching[26]. In this technique, a current is passed through the Si substrate while in the presence of a solution containing fluorine. The process for the dissolution of a silicon surface via anodic etching is displayed in **Figure 2.1**. The process can be summarized as follows:

1. Hydrogen passivated silicon remains unaffected by an HF solution without the presence of an electric current
2. When a voltage is set across the Si surface and HF electrolyte hole migrate to the surface and oxidize the Si and allow F to break the Si-H bond
3. A second F ion can then attack the remaining hydride bond causing the formation of H_2 gas which injects an electron into the Si surface
4. The Si-F bonded Si becomes more susceptible to attack by F which breaks the Si-Si bonds
5. A silicon tetrafluoride is formed which reacts with HF to from SiF_6^-, the surface returns to a neutral state until another hole migrates to the surface

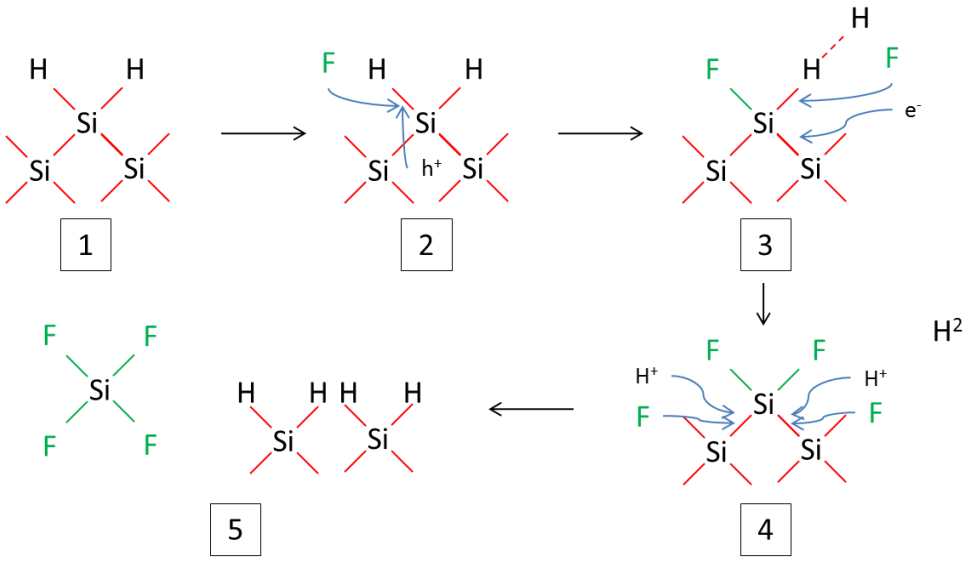

Figure 2.1 Schematic of the steps involved in the anodic dissolution of silicon

The chemical reactions are given by[27]:

Surface reaction 1: $Si(surface) + 2HF + 2h^+ \rightarrow SiF_2(surface) + 2H^+ + 4e^-$

Surface reaction 2: $SiF_2(surface) + 4HF \rightarrow H_2SiF_6(solution) + H_2$

Partial reactions: $SiF_2 + 2F^- \rightarrow SiF_4^- + e^-$ and $2H^+ + 2e^- \rightarrow H_2$

Other methods exist that do not require the use of anodization equipment, these forms of electroless electrochemical etching include metal assisted[28], chemical vapor etching, and stain etching[29]. A comprehensive review of Si porosification has been given by Korotcenkov et al.[21]. Stain etching, also known as chemical etching, is a facile method of producing nanometer scale features on silicon surfaces[30]. Fathauer et al. were the first to demonstrate a non-anodic chemical etching method for producing photoluminescent Si layers in which the porosity is created by etching single crystal Si in aqueous solutions of HF and HNO_3[31]. In

stain etching process, the holes required to dissolve the Si substrate are provided by an oxidant. The chemical reaction proceeds in three steps:

Initiation: $Si + Ox^{+} \rightarrow Si^{+} + Ox$

Etching: $Si^{+} + 3HF \rightarrow HSiF_3 + 2H^{+} + e^{-}$

Products: $HSiF_3 + 3HF \rightarrow H_2SiF_6 + H_2$

The main requirement in selecting an oxidant to etch silicon is their standard electrode potential (E_o). This parameter must be greater than the +0.7 V required to inject holes into the valence band of Si[32]. In addition to HNO_3, several other oxidants have been shown to be effective in etching Si. These include Fe(III) E_o=+0.77 V, Ce(IV) E_o=+1.4 V, and V(V) E_o=+1.0 V[30].

Pore formation in either the anodic or stain etching process may only occur if the holes are preferentially directed to the bottom of the pores. In anodic etching there are two different effects which can cause this to occur (**Figure 2.2**A). One, an inhomogeneous electric field can guide the carriers into the bottom of the pore. Two, when the pore wall becomes narrower than the exciton radius, quantum confinement effects shift the band gap. The band bending at the interface between the bulk and the pore direct the carriers to the bottom of the pore.

In the stain etching method, hole creation is controlled by the diffusion of oxidant ions to the surface of the silicon (**Figure 2.2**B). While the surface Si is being dissolved, holes get injected into the bulk at a greater rate than into the top or wall

of the pore. The thickness of the porous layer produced is self-limited by the diffusion of the oxidant through the structure[30].

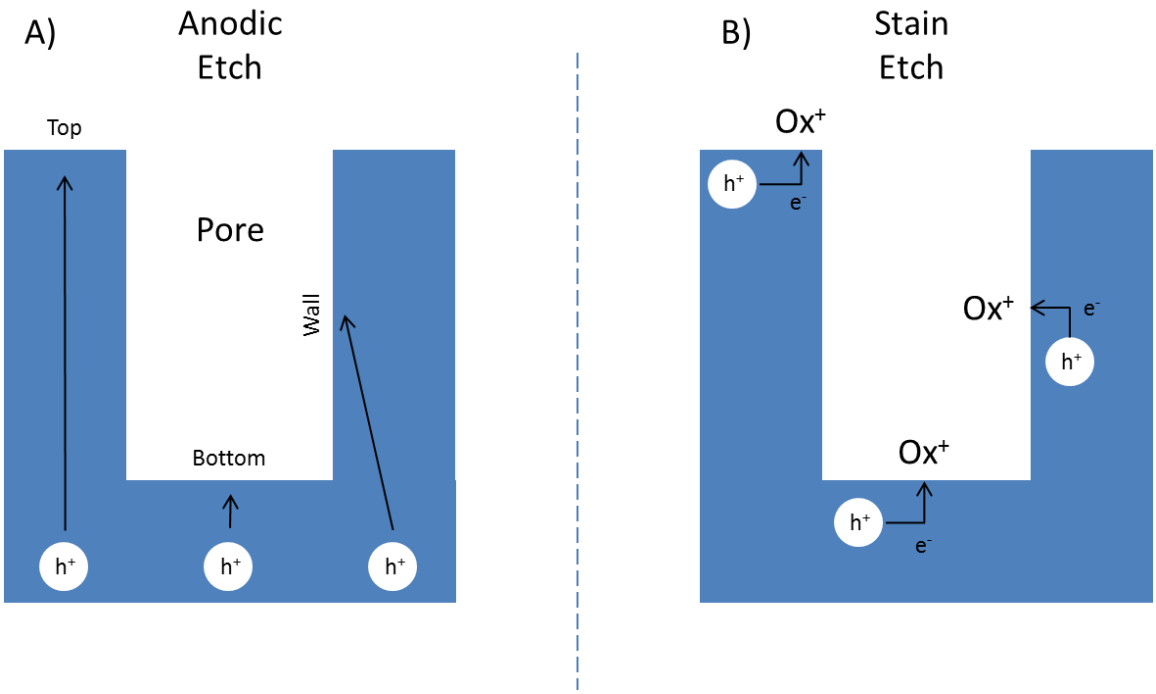

Figure 2.2 A) In anodic etching holes are created in the bulk and transported under an electric field to the reactive interface. B) In stain etching holes are created when an oxidant becomes reduced upon gaining an electron from the Si surface (adapted from ref[30])

2.3.2 Nanocrystalline Si

The two main approaches to the synthesis of nc-Si are chemical and mechanical. In general, chemical synthesis methods involve the reduction of a Si containing precursor. Several examples exist for this method, such as thermal reduction of a sol-gel glass[12], laser induced pyrolysis of silane[33], melt synthesis[34], reduction of Si containing (zintl) salts[35], and tetrachlorosilane[36]. The advantages to chemical synthesis are greater control of size, morphology, and the ability to easily

form different surface terminations. However, the drawbacks are low yields as well as having to work at high temperatures and or pressures.

Mechanical methods involve physically extracting the nc-Si from a substrate. Several examples are found in the literature, these include laser ablation[37], ball milling Si, as well as sonication to remove the nanocrystals that compose anodized[38], [39] and metal assisted p-Si films[40]. Although the methods listed are simple to carry out, they lack control of particle size and typically have low yields as well.

2.3.3 Amorphous Si

The most common methods of producing amorphous Silicon (a-Si) are through a deposition process, such as reactive sputtering, glow discharge decomposition, and plasma enhanced chemical vapor deposition (PECVD). In reactive sputtering a silicon target is sputtered by an inert gas, typically Ar, in the presence of a small partial pressure of H_2. In glow discharge decomposition a gas containing Si (e.g. SiH_4, Si_2H_6, or SiF_4) disassociates in an electric discharge and deposits on a substrate. In PECVD, silane gas is disassociated by radio frequency plasmas and the deposited onto a heated substrate. In all technique the films contain 5-25 atomic% hydrogen, with most of its properties sensitive to the concentration of hydrogen and to the parameters of the deposition[41].

Nanoparticles of a-Si have been produced via the reduction of Si in SiN films by PECVD[42] and through the reduction of silane in a non-thermal low pressure plasma reactor[43].

Photoluminescent thin films, 80 to 400nm thick, of amorphous porous silicon have been produced by Solomon et al.[44] and Estes et al.[45]. Their synthesis method consisted of depositing a-Si onto a substrate such as (111) Si, indium tin oxide, or stainless steel followed by an anodization etches in an HF containing electrolyte. An alternative method employed by Ovsyuk et al. created ap-Si films through irradiation of p-Si by $^{10}B^{+}$ ions[46].

2.4 Origin of Photoluminescence

2.4.1 Mechanisms for Light Emission

Although this topic has been researched for more than two decades, the origin of visible room temperature emission of light from nanostructured Si is still a controversial topic. Photoluminescence in porous Si was originally attributed to quantum confinement effects from nanocrystalline Si domains[20]. Later, additional theories emerged to try and explain the phenomenon. The major alternative theories are claim that the luminescent properties are a result of amorphous Si layers, surface species, or surface molecules. In this section we will briefly discuss each of these models.

2.4.1.1 Quantum Confinement

The electronic properties of semiconductor materials change drastically when their dimensions become spatially confined. When quantum confinement effects occur, the band gap of a semiconductor increases with a decrease in size. Fluorescent emission in these systems is defined by the radiative recombination of excitons through the band gap. Consequently, a decrease in the size of a nanocrystal will

result in a blue shift in the emission. Several groups have presented evidence of size tunable emission in nc-Si[24], [47–50]. However, it has also been shown that other properties also contribute to its optical properties of nano-structured Si in addition to quantum confinement[51]. Assigning the emission process exclusively to quantum confinement effects may not accurately represent the emission process.

2.4.1.2 Surface Species and Molecules

When the volume of a structure is reduced its surface to volume ratio increases. As a result, surface properties provide a greater contribution to the optical properties of a material. In p-Si and nc-Si, structures are on the order of nanometers giving them high surface areas with various chemical ligands such as silicon hydrides, oxidized hydrides, oxides, and others which attach to the unsatisfied chemical valences on the Si surface. Adjustments to the surface cause bond angle and bond length variations among the Si atoms. The result is a spectrum of electronic states in which the elementary excitations are localized on a length scale similar to hydrogenated a-Si. Localized changes of the wave function would provide a number of trapped states which carriers can then radiatively recombine by a tunneling mechanism. Recombination between the disordered-induced localized states may account for the fluorescent emission[52].

The recombination mechanism in oxidized nanocrystallites in nc-Si and p-Si is different from that found in ones passivated by hydrogen. It has been claimed to be responsible for both blue shifts[53] and red shifts[54] in fluorescent emission.

Hydroxyl groups adsorbed on oxidized Si in p-Si have also been claimed to be responsible for the observed green/blue emission[55].

It has been demonstrated that the emission in nc-Si is sensitive to its interfacial states[56], [57]. A three region model for p-Si has been proposed in which interfacial region plays an important role in the emission process[58]. The three regions are composed of a crystalline core, an outer oxide layer, and an interfacial layer between the first two. The a-SiO_2 surface regions form a high potential barrier which confines excitons within it. Photogenerated excitons are created in the c-Si core. Radiative recombination occurs when the photogenerated excitons from the core region become localized to the interfacial layer between the core and the oxide layers.

Siloxene ($Si_6O_3H_6$) is a molecule that has been proposed as the emitting material in p-Si[59]. It is composed of a mixture of six member rings of Si interconnected by oxygen and saturated by H and OH. FT-IR and Raman analysis of this molecule showed quite similar vibrational properties to p-Si. Photoluminescent properties were also comparable[60]. It is believed that this molecule may be present on the surface of p-Si as a result of anodized or chemical etching[61].

2.4.2 Emission in Amorphous Si

Before discussing the emission mechanisms in amorphous Si, it is a good idea to review some electronic properties of a-Si. In crystalline semiconductors, an electron's wavefunction can be described as a Bloch wave, due to the periodicity of the electron's potential energy within the crystal. This wavefunction forms

extended states which are present throughout the crystal. As a result, the electron is a part of the whole crystal; it has equal probability of being found in any unit cell. The wavevector (k) behaves as a quantum number. Interactions between an electron and external forces, photon, or phonons can be described by a momentum ($\hbar$k). In the case of a-Si, due to the lack of long range order, the Bloch wavefunction cannot be used to describe the electron. As a result we cannot use the wavevector (k) or the momentum ($\hbar$k) to describe the electron's motion[62]. Nevertheless, a-Si does have short range order and thus possess an energy gap between its valance and conduction band.

Figure 2.3 compares the differences in localizes and extended states found in a-Si. The potential energy of the electrons in amorphous semiconductors varies significantly from one site to another. Some locations within the structure can have strong local changes in its potential energy, caused by defects such as variations in bond lengths or over/under coordinated atoms. Such locations in the material can form finite potential wells. These locations trap electrons to a particular spatial location by giving them localized wavefunction, known as localized states (**Figure 2.3**C). Electrons in amorphous silicon also have electrons that belong to the whole solid; these electrons possess extended wavefunctions and are known as extended states. These extended states differ from those found in the crystalline phase due to their random potential fluctuations. The extended and localized states are separated by the both the conduction band (E_c) and the valance band (E_v) (**Figure 2.3**A). States that exist within the mobility gap are a result of either tail

states or defects (**Figure 2.3**B). Tail states are due to the structural disorder, variations in bond angles and lengths. Defects states exist as a result of structural defects, which could be dangling bonds, dopants, or under/over coordinated atoms in the structure[62].

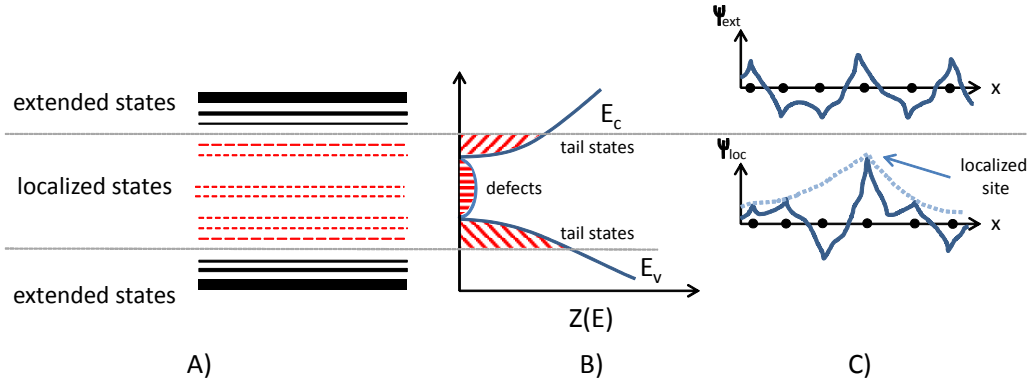

Figure 2.3 Schematic representation of the A) band structure B) density of states Z(E) C) wavefunctions of the extended and localized states in a-Si. (adapted from ref. [62])

Fluorescent emission in a-Si has been known for quite some time. At low temperatures intrinsic bulk amorphous silicon is highly luminescent with quantum efficiency in the order of 10%. At temperatures less than 80 K, light emission from a-Si have been reported by various groups, with energies ranging from 0.7 up to 1.5 eV[41]. According to the commonly cited model of recombination in hydrogenated a-Si proposed by Street[41], defects provide dominant recombination centers when the temperature is higher than 100K. At low temperatures, photogenerated carriers thermalize in the tail states and become trapped. These excitons can then recombine either radiatively if sufficiently distant from a defect center, or non-radiatively if captured by a defect.

Amorphous regions have also been observed in luminescent chemically etched p-Si[63] and have been claimed to be the source of light emission. Due to the presence of these complex electronic structures, providing an exact model of light emission in ap-Si is quite challenging. Nanostructured amorphous porous Si films synthesized and studied by Bustarret et al.[64], Wehrspohn et al.[65], and Estes et al.[66] help give some insight into the emission process in this class of materials.

When excitons are created in a-Si, they thermalize to the band tails and become trapped in localized states. These electron-hole pairs can now either radiatively or non-radiatively recombine. The probability of radiative recombination is determined by its distance from a defect. A non-radiative capture radius R_c can be defined around a defect and is given by equation 1.

$$\boldsymbol{R_c = \frac{R_0}{2}\ln(\tau_0 \omega_0)} \qquad \textbf{(1)}$$

Here R_0 is the localization radius, τ_0 is the radiative lifetime, and ω_0 is the attempt to escape frequency ($\sim 10^{12}$ Hz). R_c is typically in the range of 10 to 12 nm with a R_0 of about 10Å. This means that if an exciton is created outside this capture region given by a sphere of volume, $V_c = 4\pi R_c^3/3$, radiative recombination can occur. **Figure 2.4**A illustrates the role of non-radiative capture regions in a-Si. A majority of the space is occupied by these regions, leading to negligible emission at room temperatures. However, when bulk a-Si is etched into nanoporous structures with characteristics sizes smaller then R_c, the probability of encountering a non-radiative center is no longer given by V_c, but by the intersection of V_c with the nanostructure. As shown in

Figure 2.4B, the non-radiative capture regions become truncated or removed from the etched material, resulting in an increase in quantum efficiency. This method of emission in ap-Si is known as the spatial confinement model[67].

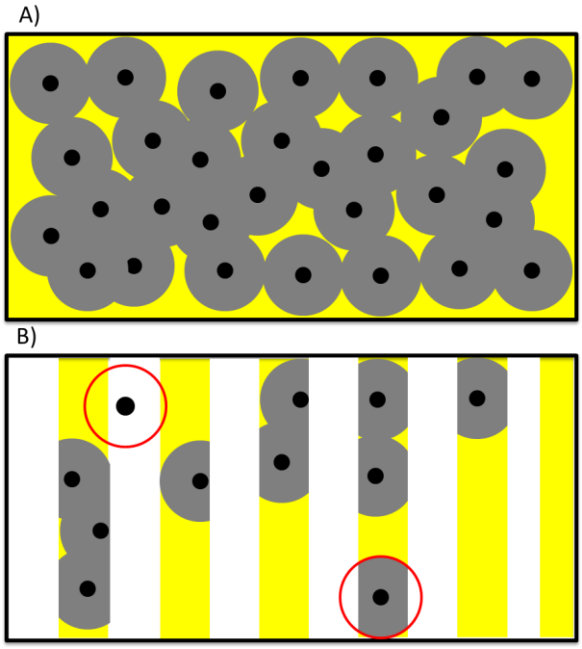

Figure 2.4 Schematic of spatial confinement in ap-Si A) bulk a-Si and B) ap-Si, black dots represent non-radiative centers dark grey circles represent non-radiative capture regions, yellow regions are radiative, and white areas are void of material (adapted from ref.[68])

2.5 Summary

Nanostructured Si is an interesting material for both the viewpoints of fundamental physics and device applications. There exist numerous methods to create nanostructured Si. The most well studied being nc-Si and p-Si. Although much is known about this material, the precise origin of light emission is still a topic of debate in the literature. Several models have been proposed to describe the mechanism, but none have been accepted as the definitive model. Differences in synthesis techniques, characterization methods, and results lead to a confusing

array of contradictory conclusions. Nevertheless, the importance of studying Si in these forms is crucial for applying this material in the next generation of devices and products.

In the next chapter we will discuss the materials and methods used during the course of our research.

3 EXPERIMENTAL METHODS

3.1 Introduction

The primary goal of this research was to develop a method for creating colloidal suspensions of nanostructured Si and characterize both their physical and optical properties. The experimental methods were designed to determine the most effective etchant formulation and processing procedure for the synthesis of this material. Etchant formulations were selected based on a review of existing literature related to the porosification of Si substrates via electroless electrochemical etching. The most common materials used for this research are listed in **Table 3.1**. Solvents such as ethanol, isopropanol, and toluene were degassed prior to use. This was accomplished by placing them in a vacuum desiccator and stirring the solution with a stir bar and magnetic stirring plate. Porous Si films were characterized through Scanning Electron Microscopy (SEM) and Transmission Electron Microscopy (TEM). After removing these films via sonication, the resultant suspensions were studied using several types of characterization methods. The materials and characterization methods used during this research will be discussed in this chapter.

Table 3.1 Materials used in the synthesis of nanostructured Si

Material	Manufacture	Description
Silicon, Si	Addison Electronics	(100), p-type, B-doped, 1-10 Ωcm
Hydrogen Fluoride, HF	Fluka	49 vol% Trace select ultra
Nitric Acid, HNO_3	Fluka	70 vol% for trace analysis
Hydrochloric Acid, HCl	Fischer Scientific	35 vol%
Iron(III) Chloride, $FeCl_3$	Fischer Scientific	$FeCl_3$ $6H_2O$ hexahydrate
Ethanol, C_2H_6O	Sigma Aldrich	ACS reagent grade 99.5%
Isopropanol, C_3H_8O	Fluka	Chromosolve grade 99.8%
Toluene, C_7H_8	Fischer Scientific	ACS 99.5%
Distilled Water, H_2O	Millipore Milli-q	ρ -18.2 Ωcm

3.2 Synthesis of Stain Etched Nanocrystalline Si

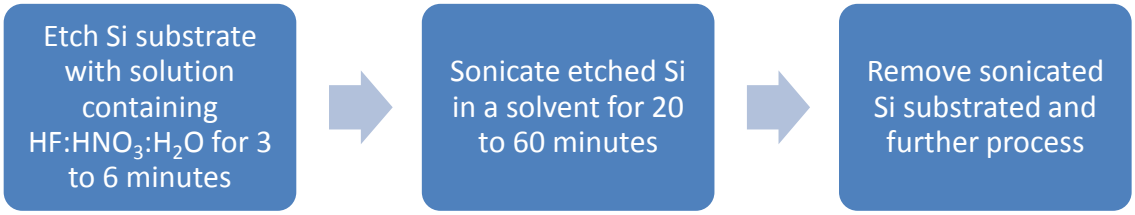

Figure 3.1 Outline of the synthesis process for producing nc-Si suspensions

Nanocrystalline Si (nc-Si) was synthesized from p-type (100) boron doped Si wafers. **Figure 3.1** summarizes the process for producing nc-Si suspensions. Since the oxidant in this process, NO^+, has a standard electrode potential of + 1.45 V[69], it meets the conditions for electroless etching Si, E_o > 0.7 V. The synthesis method involves two basic steps. The first is to create a nanoporous crystalline layer which is then removed through a sonication step dispersing the nanocrystals into a solvent. Si wafers were cut into 2.5x4.5 cm strips and submerged in a dilute HF solution (50:1 by volume HF:H_2O) to remove the native oxide layer prior to

submergence into the etchant. The etching solution was composed of HF: HNO3:H_2O mixed in a 4:2:5 volume ratio. The etching of Si in this mixture is autocatalyzed by HNO_2 which requires a quiescent period of several minutes before significant etching arises. In order to reduce this induction time, the Si strips were briefly dipped into a solution containing only the HF and HNO_3 prior to it being diluted with the deionized water[31]. Si strips were then submerged into this solution for 3 to 6 minutes. In a typical reaction 8 Si strips were submerged in 60ml of etching solution, using two 30 ml Teflon beakers. It was found that longer reaction times created violent reactions which emit brown gases of what could be NO_x as well as cause the solution to heat and effervesce.

After reacting the Si strips were rinsed with ethanol, isopropanol, or methanol and dried under a N_2 stream, before being placed into a sealable vessel containing the desired solvent. Stain etched Si exhibited a browning blue coloration on the surface. The solvent containing the Si strips was then sonicated using an ultrasonic bath (VWR) for between 20 to 60 minutes. Sonicating p-Si films produces cavitations on the surface which upon collapsing can create shock waves. This action provides the necessary energy to remove the particles from the surface[39]. After sonication, strips were removed from the solvent and either stored or re-etched and sonicated to further increase the concentration of nc-Si in the solvent. A schematic of the process is displayed in **Figure 3.2**. The remaining solution now contained both nc-Si as well as larger aggregates porous Si. Two methods were employed in order to separate these two components. The solutions were either centrifuged at 10,000

rpm for 10 min or strained through either a 200 nm or 400 nm PTFE filter membrane.

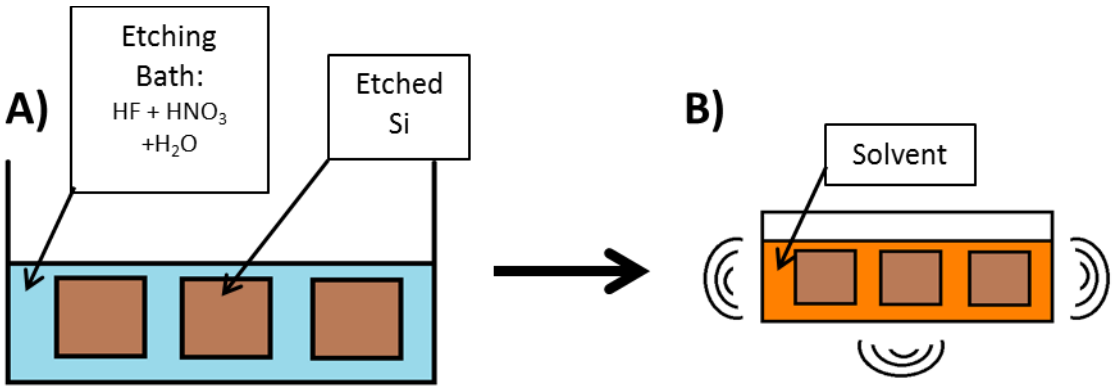

Figure 3.2 Schematic representation of the synthesis procedure A) etching Si in etching bath B) sonicating etched Si to remove porous layer

Since this etching method could be performed on arbitrarily shaped object, attempts were made to employ this method to create nc-Si using powdered Si. Small Si particles have a greater surface to volume ratio and therefore should yield higher concentrations of nc-Si. Si powders were prepared by ball milling Si wafers. These powders were then reacted with the etching solution, and removed from the etchant through filtration, prior to rinsing and sonication. Although there was some success with this method, the difficulty in handling the powders forced us to abandon this approach.

3.3 Synthesis of Stain Etched Amorphous Porous Si

Figure 3.3 Outline of the synthesis process for producing ap-Si suspensions

As seen in **Figure 3.3**, the synthesis of amorphous porous silicon (ap-Si) was very similar to that of nc-Si, the main difference being the choice of etching solution and the etching time. As discussed in the chapter 2, various oxidizing agents can be employed to create porous Si layers on Si substrates. One such oxidant is iron (III) chloride, $FeCl_3$. For our work, We selected an etchant composition similar to one reported by Dudley et al[70]. It was a mixture of 0.48M of $FeCl_3 \cdot 6H_2O$ combined with a 7:3 volume ratio HF:HCl solution. A typical synthesis involved mixing 7.8g of $FeCl_3 \cdot 6H_2O$ into a solution containing 43ml of HF and 18ml of HCl. Below are the chemical reactions for this process:

Cathode: $Fe^{3+} \rightarrow Fe^{2+} + h^+$

Anode: $Si + 6HF + h^+ \rightarrow H_2SiF_6 + 4H^+ + 3e^-$

Overall: $Si + Fe^{3+} + 6HF \rightarrow H_2\,SiF_6 + Fe^{2+} + 4H^+ + 3e^-$

The role of the HCl is to acidify the iron (III) chloride in solution in order for it to maintain its solubility. It was also shown to decrease the induction time for the

etching reaction[71]. The oxidant, Fe^{3+}, has a standard oxidation potential is +0.77 V, meets the requirement for stain etching Si (E_o > 0.7 V).

In this reaction 8 Si strips were submerged in 60ml of etching solution, using two 30 ml Teflon beakers. After the Si strips were placed into the etching solution, it took approximately one minute for the reaction to begin. Certain regions of the Si surface began to turn purple, but as the reaction proceeded the surface turned brownish black. The reaction was allowed to continue for 15 to 20 hours before the Si strips were removed. At the end of the reaction a white precipitate with yellow or green hues formed on the edges of the Si strips as well as the bottom of the beaker. This precipitate may be hexafluorosilicic acid, H_2SiF_6, which precipitate out of solution due to over saturation.

The Si strips were cleaned by first dipping it in a solution of deionized water and then rinsing in ethanol. They were then dried under a nitrogen stream until any remaining ethanol was removed. During this drying procedure the surface of the Si strips exhibited a matte brownish yellow appearance, which was easily removed through gentle mechanical abrasion. These etched and dried substrates were then placed into a solvent such as ethanol or toluene and sonicated in a closed container placed in a sonicating bath for 30 minutes. Again, sonicating these ap-Si films produces cavitations which upon collapsing create shock waves on the surface. This action provides the necessary energy to remove the particles from the surface[39]. The Si strips were then removed from the sonicated solution. This sonication step removed the yellow surface and exposed a matte black inner layer of the Si

substrate. The solution which now contained the yellow top layer was further sonicated to reduce the size of the ap-Si particles. We processed the solution using an ultrasonicating horn, Q500 (Q Sonica), set at 40% amplitude with a tapered tip for an additional 30 minutes. This step created a finer particle size which allowed it to stay in suspension for a longer period of time.

3.4 Characterization

3.4.1 Introduction

In these sections we briefly review the fundamental principles of the various characterization techniques employed in this research. We also explain how samples were prepared for each technique.

3.4.2 Morphology

3.4.2.1 Scanning Electron Microscopy

A Nova NanoSEM 50 scanning electron microscope (FEI) was used to study the morphology of stain etched Si surfaces as well as ap-Si particles. SEM is a widely used imaging technique that involves the use of a beam of high energy electrons to scan the surface of a given sample. The interaction between the sample and the impinging electron beam provides insight into the morphology, topography, and composition. The major signals generated in an SEM include secondary electrons, back-scattered electrons, and characteristic X-rays. Secondary and back scattered electrons are the primary signals used to image a specimen. With a resolution of 1.8nm and a depth of field of 4μm, it is one of the best means of understanding

materials at the micron and nanometer scales[72]. For our measurements the beam voltage was set to 2 keV.

Samples were prepared depending on their composition. Etched Si substrates were cleaved into approximately 1x2cm pieces using a diamond tipped scribe, after which they were attached to an aluminum specimen mounts using either carbon, copper, or aluminum tape. Powder samples were scattered on copper tape or directly on to an aluminum specimen mount.

3.4.2.2 BET Porosimetry

BET porosimetry was used to measure surface area and pore size distributions of ap-Si samples. We conducted our measurements on an ASAP 2420 surface area and porosimetry system (Micrometrics). This method involves the physical adsorption of gas molecules, adsorbate, on the surface of sample, adsorbent. This adsorption process is usually described through isotherms, which refer to the amount of an adsorbate present on an adsorbent as a function of its pressure at a constant temperature.

Brunauer-Emmett-Teller (BET) theory was used to determine the surface area and pore size distribution of our material. BET theory is used to describe multilayer molecular adsorption and is an extension to the Langmuir theory for monolayer adsorption. The total and specific surface areas can be calculated using equation 2 and 3 respectively. Here v_m is the monolayer of adsorbed gas, N is Avogadro's number, s is the adsorption cross section of adsorbing material, V is the molar volume of the adsorbate gas, and a is the mass of adsorbent[73].

$$S_{BET,total} = \frac{v_m \cdot N \cdot s}{V} \qquad (2)$$

$$S_{BET,specific} = \frac{S_{BET,total}}{a} \qquad (3)$$

Samples were prepared by completely evaporating the solvent under vacuum and degassing through heating the sample to 200°C in a N_2 environment. Physical adsorption tests were carried out at -195.8°C using N_2 as the analysis adsorptive.

3.4.2.3 Atomic Force Microscopy

Atomic Force Microscopy (AFM) was briefly used to measure the dimensions of ap-Si particles. We used a 5400 Scan Probe Microscope (Agilent Technologies) under contact mode for our studies; the tip used was a NT-MDT CSG01 with a 10 nm tip radius. The AFM uses a cantilever with a sharp tipped end to scan the surface of a specimen. When the tip is brought on to the surface, the forces between the tip and the sample lead to the deflection of the cantilever. Various forces can be measured by these deflections, such as van der Waals forces, chemical bonding, and electrostatic forces. Deflections of the cantilever are measured through the displacement of a laser spot reflecting from the top surface of the cantilever onto a photodiode array[72]. Using this method we were able to image and measure topographical features of ap-Si particles.

Samples were prepared by depositing suspensions of ap-Si onto a (100) silicon substrate and drying off the solvent under vacuum.

3.4.3 Structural

3.4.3.1 Transmission Electron Microscopy

Transmission electron microscopy (TEM) is one of the most versatile tools available to characterized nano-scaled materials. Its versatility lies in the fact that it can be used to study various aspects of a material at nanometer dimensions. TEM operates by using the wave properties of electrons as it passes through an ultra-thin section of a material. Sample thicknesses can range from a few nanometers up to approximately 500 nm, depending on the elemental composition of the material as well as the energy of the incoming electron beam. The electrons are first generated using a field emission gun, they then pass through a series of apertures and condenser lenses which create a coherent beam which interact with a material in several ways. In our work we used the TEM to conduct high resolution TEM (HRTEM), Scanning TEM (STEM), energy dispersive spectroscopy (EDS), and selected area electron diffraction (SAED). In STEM a highly focused narrow spot electron beam rasterizes over a sample. This method was used to obtain high Z contrast images. EDS uses secondary electrons to determine the elemental composition of the sample material. It was used to determine elements present on the nanostructured Si. SAED provides a diffraction pattern of the material being sampled[72].

Samples were prepared by depositing 1-3 μl of a sample solution onto a carbon coated Cu 300 mesh TEM grid. The solutions were then allowed to dry in air or blotted using filter paper. The blotting process is intended to rapidly remove the

solvent from the grid, but it was observed that the deposited sample also was removed with this process. The grids were then either placed into the TEM or further treated with plasma consisting of 25% O_2/75% Ar in order to remove any residual solvent molecules remaining on the surface. It was found that plasma treatments reduced the amount of surface contamination during high resolution imaging and STEM imaging. The carbon coatings on the grids were either ultrathin or holey carbon film. Graphene coated Cu 1000 mesh were also used to examine Si nanostructures. These grids did not show any improvement in image quality, and exhibited diffraction spots in SEAD.

3.4.3.2 Raman Spectroscopy

We used Raman spectroscopy to help determine the phase of ap-Si. In our experiments we used a LabRam ARAMIS Raman spectrometer (Horiba) equipped with a 473 nm 6 mW cobalt laser. Raman spectroscopy is used to study low-frequency modes in a material, through the inelastic scattering of monochromatic (laser) light. Phonons become excited by the incoming laser photons and shift its energy either up or down. This shift in energy gives us information about the vibrational modes of a material[74].

Samples were prepared by evaporating the solvent from the ap-Si suspension and depositing the dried powders on a glass slide. It was found that the sample was sensitive to the laser intensity. This could be seen through an optical microscope as a discoloration as well as changes in the Raman spectrum with longer exposure times. Laser intensity was controlled through apertures and filters, while exposure

times were minimized as to not damage the samples during measurements. For most experiments we used a D1 filter (0.6 mW laser intensity), a 100 μm aperture, and an exposure time of 30 seconds.

3.4.4 Chemical Composition

3.4.4.1 X-ray Photoelectron Spectroscopy

An Axis Ultra DLD X-ray photoelectron spectrometer (Kratos Analytical) was used to study the composition and phase of ap-Si powders. X-ray photoelectron spectrometry (XPS) is an ideal tool for studying the elemental composition as well as chemical and electronic states of the elements found on the top most (1-10 nm) surface of a material. It has the ability to detect all elements with an atomic number of 3 (Li) and above. This technique measures the binding energies of electrons in a given material. X-ray photons of a particular wavelength/energy strike the surface of a material and interact with the atoms at or near the surface causing it to eject electrons. Since the X-ray energy is known, the electron binding energy, $E_{binding}$, of every emitting electron can be calculated using equation 4.

$$\mathbf{E_{binding} = E_{photon} - (E_{kinetic} + \Phi)} \qquad \mathbf{(4)}$$

Where E_{photon} is the energy of the incoming X-ray, $E_{kinetic}$ is the kinetic energy of the electron and Φ is the work function of the spectrometer. Each element has its own characteristic energy peaks[72].

XPS samples were prepared by evaporating the solvent from ap-Si suspensions under vacuum and then depositing the dried powder onto a 1x2 cm strip gold

coated glass substrate. We used a monochromatic Al Kα X-ray source operating at 150 W, a multi-channel plate and delay line detector under 1.0 x10-9 Torr vacuum.. All spectra were recorded using an aperture slot of 300 μm x 700 μm, survey and high-resolution spectra were collected at fixed analyzer pass energies of 160 and 20 eV, respectively. Binding energies were referenced to the C 1s binding energy of the carbon contamination which was taken to be 284.8 eV.

3.4.4.2 Fourier Transformed Infrared Spectroscopy

For our Fourier transformed infrared spectrometry (FT-IR) measurements we used a Nicolet iS10 (Thermo Scientific) FT-IR spectrometer. FT-IR is a powerful yet simple tool to use for studying chemical bonding in a material. It is a type of absorption spectroscopy similar to Raman spectroscopy. In this technique infrared (IR) light passes through a beam splitter which splits the incoming light into two beams that then recombine out of phase producing an interferogram. This interferogram signal contains all the information for every infrared signal emitted from the source. This signal passes through the sample and in the process certain frequencies get absorbed by the material. The interferogram signal leaving the sample now contains information regarding the IR absorbance of the sample. [75]. Computer processing is required to convert this signal, collected by photodetector, into readable results through the use of a Fourier transform. The infrared spectra that are produced are a result of the absorption of electromagnetic radiation at frequencies corresponding to the vibration of specific types of chemical bonds found

on or within a material. More information regarding this technique and its application for studying Si bonding vibrations can be found in appendix 8.1.

Several methods were employed in preparing samples for FT-IR. Initially we tried to study samples dispersed in solvents using a liquid sample holder. However, this method did not yield expectable results since the signals generated by the solvent itself masked any signal from our samples. We next tried to use the method most cited in the literature, which consists of drop casting the liquid sample (0.1 ml) onto a KBr pellet and taking measurements after evaporating the solvent. This method showed better results than the first, but the signals measured were still weak, and contained a lot of background noise. The final preparation method we employed consisted of drying 1 to 2 ml of a sample in a micro centrifuge tube containing 0.1g of either KBr or NaCl powder under vacuum or using a rotary evaporator (Labconco). The powder loaded with the samples was then processed into pellets used for measurements. The last method yielded the best and most consistent results.

3.4.5 Optical

3.4.5.1 Fluorescence Spectroscopy

For our photoluminescent emission (PL) and excitation (PLE) experiments, we used a Fluoromax-4 spectrofluorometer (Horiba). Fluorescent materials can be studied using this method due to the fact that they contain discrete electronic states which an electron can occupy. When an electron is excited from a ground state to an excited state through the absorption of a photon, it can then radiatively relax back to

its initial state through the emission of a photon[76]. Typically, excitation wavelengths are in the ultra violet 330 to 380 nm, while emission ranged through the visible wavelengths. PL is measured using a fixed excitation wavelength and scanning a range of emission wavelengths. PLE is measured by fixing an emission wavelength and scanning a range of excitation wavelengths. 3D contour maps can also be created in which both excitation and emission are measured with respect to intensity. Excitation and emission intensity were controlled through the use of adjustable slits. These slits were typically kept at 5nm, but were reduced if there was any saturation in intensity. Second order emission from the excitation wavelengths were filtered by using either a 375 nm or 399 nm high pass filter. Temperature effects were measured using a temperature controller and a Peltier sample holder module.

PL lifetime measurements were conducted using a F900 spectrometer (Edinburgh Instruments). We measured the lifetimes of our samples through a time correlated single photon counting (TCSPC) method. Samples were excited at their peak emission wavelengths using a nanosecond Xe flash lamp. Intrinsic lifetime parameters are determined through a numerical analysis procedure. The decay process is typically modeled as an exponential decay, given by eqn. 5

$$\mathbf{R(t) = A + \sum_{i=1}^{4} B_i e^{-\frac{t}{\tau_i}}} \qquad \mathbf{(5)}$$

Where A is an additional background (i.e. the excitation source), B_i is a pre-exponential factor, t is time, and τ is the radiative lifetime. Radiative lifetime

expresses the time it takes to decay from the beginning of the decay to a level of about 37% of the original value. Typically lifetime measurements can be fitted to three exponential terms. The average lifetime of the entire decay process is given by eqn. 6

$$\boldsymbol{\tau_{avg}} = \frac{B_1\tau_1^2+B_1\tau_2^2+B_1\tau_3^2}{B_1\tau_1 +B_1\tau_2 +B_1\tau_3} \qquad \textbf{(6)}$$

Sample preparation involved transferring a sample solution into either a standard 3 ml quartz cuvette or a 0.5ml quartz micro cuvette. Samples for temperature dependence measurements were kept stirred using a small magnetic stir bar which was placed in a 3ml cuvette.

3.4.5.2 Absorbance Spectroscopy

Absorbance measurements were carried out using a Genysis 10S UV-Vis Spectrometer (Thermo Scientific). Information regarding materials electronic transitions, its band gap, or its excitonic absorbance peak can be determined using this method. This technique involves measuring the absorbance of radiation as a function of wavelength. A range of monochromatic light is directed at a sample and a photodetector is placed across from the source and sample, in order to measure which wavelengths transmit through. Absorbance values are calculated using equation 6, where A is absorbance, P_0 is the intensity of the monochromatic light, and P is the intensity of transmitted light. [76]

$$\mathbf{A = \log_{10}\frac{P_0}{P}} \qquad \textbf{(6)}$$

Absorbance spectrums were measured from deep UV (200nm) through the visible (800nm).

Samples were prepared by placing 3ml of sample solution into a quartz cuvette. Absorbance measurements for ap-Si suspensions were conducted on centrifuged samples. Non-centrifuged samples contained large ap-Si particles which scattered too much light for proper measurements. Samples were centrifuged at 500 rpm for 3 minutes in order to separate the larger aggregates.

3.4.6 Yield

Measurements of synthesis yields were conducted through gravimetric analysis. 1 ml of ap-Si solution was transferred into a 1.5 ml micro centrifuge tube and allowed to dry under vacuum or with the assistance of a centrivap rotary evaporator (Labconco). The weight of the micro centrifuge tube was measured using an XP205 weighing balance (Mettler Toledo) before and after the sample was added/dried, for which a difference was assumed to be from the synthesized materials.

3.5 Summary

The synthesis of nanostructured Si through chemical etching is a fairly straightforward procedure. However, developing the proper sample preparation protocols for characterizing the resulting products proved to be more difficult. For nc-Si, characterization methods such as Raman spectroscopy, XPS, and AFM were unavailable due to the low yields. For ap-Si, the characterization procedures were fairly simple and yielded results quickly. Since Si oxidizes in air, steps were taken to

reduce its exposure. Solvents were degassed and samples were stored in a nitrogen environment. Even with these precautions chemical analysis results may deviate from ideal conditions due to exposure to ambient air during preparation and handling.

The subsequent two chapters will present the results the results of our experiments with the two different etching methods as well as discuss their significance.

4 RESULTS AND DISCUSSION: Stain Etching with HNO_3 (nc-Si)

4.1 Introduction

In this chapter we will report and discuss the results of our work on synthesizing nc-Si particles using a stain etching process. Although the synthesis procedure for this material was fairly simple, analysis proved to be more complicated. We were limited in the range of characterization techniques available to us due to low yields. Nevertheless, the observations carried out on this material produced interesting results. In the following sections we will discuss our analysis of the material's structure through TEM, optical properties through fluorescence spectroscopy and UV-Vis absorbance, as well as chemical composition through IR absorbance and EDS.

4.2 Stain Etched p-Si Films

Following the procedure outlined in chapter 4, we synthesized fluorescent p-Si films on crystalline Si substrates using HF and HNO_3. The etched substrates were blue/purple under ambient light, and as indicated in **Figure 4.1**, PL emission measurements of these films exhibit peak intensity at 622 nm. This value is similar to what is typically reported for this etching technique[77].

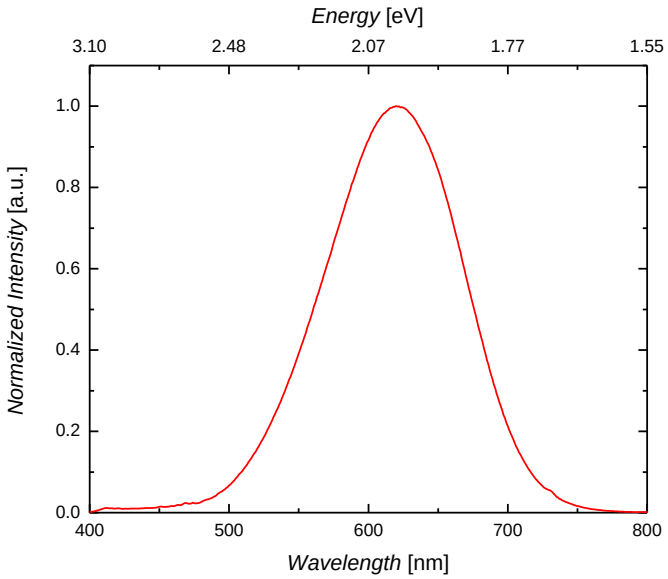

Figure 4.1 PL emission of p-Si surface

SEM imaging was conducted on these films and is displayed in **Figure 4.2**A; it shows that the surface of the p-Si is composed of a nanoporous structure with varying pore sizes and shapes. **Figure 4.2**B presents the TEM cross section of a portion of this film. It shows that the porous structure is composed of nanocrystallites of Si with lattice spacings of 3.1 Å, 1.9 Å, and 1.6 Å corresponding to the (111), (220), and (311) lattice planes of diamond cubic Si. These nanocrystallites were found to be surrounded by an amorphous phase. This amorphous phase was composed of amorphous Si and amorphous SiO_2. The SiO_2 is mainly due to oxidation during sample preparation, whereas the amorphous Si phase is believed to be a result of the etching process[31], [78].

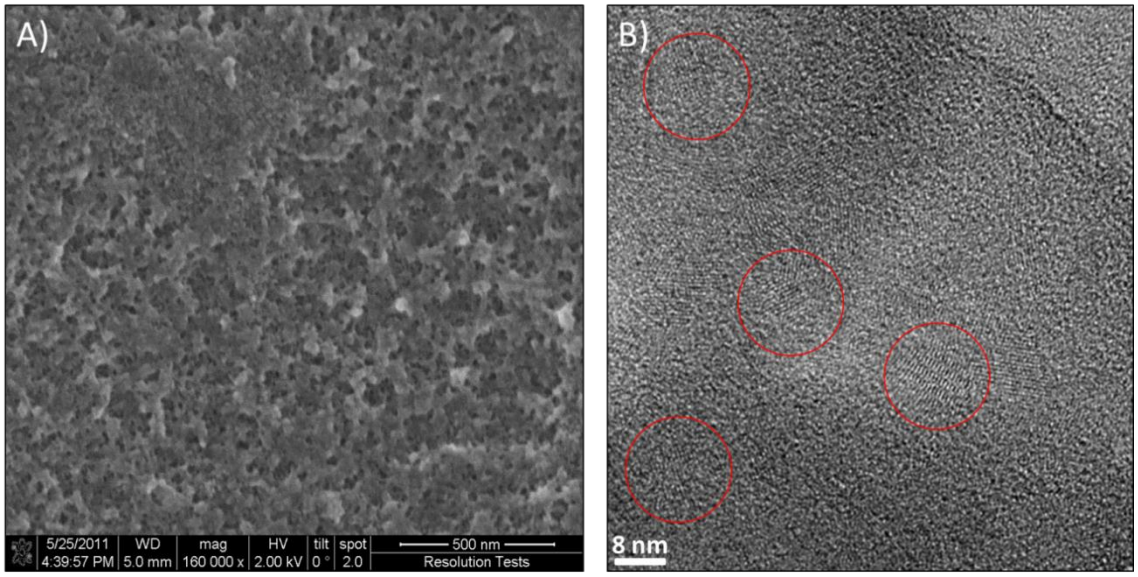

Figure 4.2 A) SEM micrograph of the surface of an etched Si substrate, B) HRTEM image of the etched Si surface (crystal domains are circled red to help guide the eye)

4.3 nc-Si from p-Si Films

nc-Si were extracted from stain etched p-Si films via sonication. STEM, **Figure 4.3**A, and HRTEM, **Figure 4.3**B, images show that nanocrystals can indeed be created through this synthesis approach.

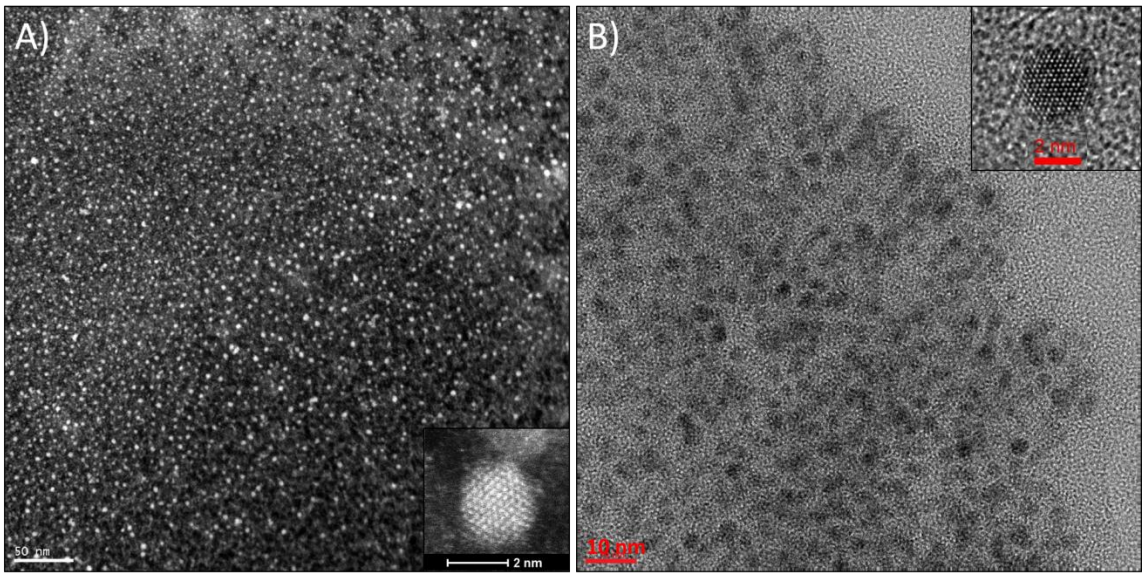

Figure 4.3 A) STEM image of nc-Si particles (inset: one nanocrystal with atomic resolution), B) HRTEM image of nc-Si particles (inset: one nanocrystal with visible lattice fringes)

Figure 4.4A presents the particle size distribution analysis that was carried out on these samples. With a count of 361 particles, it was determined that the average diameter was about 3.5 nm with a standard deviation of 0.79 nm. An EDS spectrum taken of these particles indicates that they are composed mainly of Si and O. In the EDS spectrum, signals from Cu and C are believed to be a result of using a TEM grid made of holey carbon film deposited on a Cu, shown in **Figure 4.4**B.

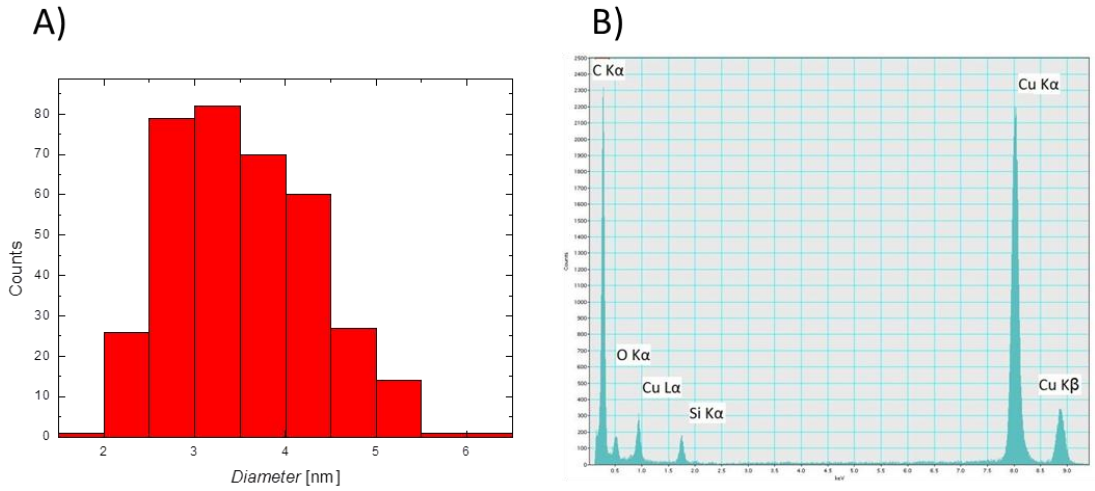

Figure 4.4 A) size distribution of nc-Si from TEM analysis, B) EDS spectrum of nc-Si

Fast Fourier Transforms (FFTs) of TEM images were taken in order to determine the lattice spacing of the nanocrystals.

Figure 4.5 presents FFTs of selected areas in a TEM image of nc-Si. 1.8 Å and 2.1 Å were the most common lattice spacings measured using this method. Typical lattice spacings found in nc-Si are 3.1 Å corresponding to the (111) plane in diamond cubic Si and 1.9 Å corresponding to the (221) plane[33]. The measured spacings are similar to those found in Cu, quartz SiO_2, the hexagonal phase of Si, as demonstrated in **Table 4.1**.

Table 4.1 Comparison between observed lattice spacings and that of different materials; numbers in parenthesis correspond to the associated plane

Recorded spacings (Å)	Si diamond cubic(Å)	Cu FCC(Å)	αSiO$_2$ trigonal(Å)	Si hexagonal
2.1	3.14 (111)	2.07(111)	2.13(200)	2.27(102)
1.8	1.92 (221)	1.79(200)	1.81(112)	1.76(103)

This difference in observed spacings, and the known values may be a result of one of three causes:

1. The TEM grids may have been contaminated with Cu nanoparticles. Alternatively, Cu from the grids has been dissolved by residual acids in the sample solution and reduced on the carbon to form Cu nanocrystals.
2. These nanocrystals may have been composed of a different crystalline phase of Si.
3. The Si has been oxidized into a quartz phase of SiO_2.

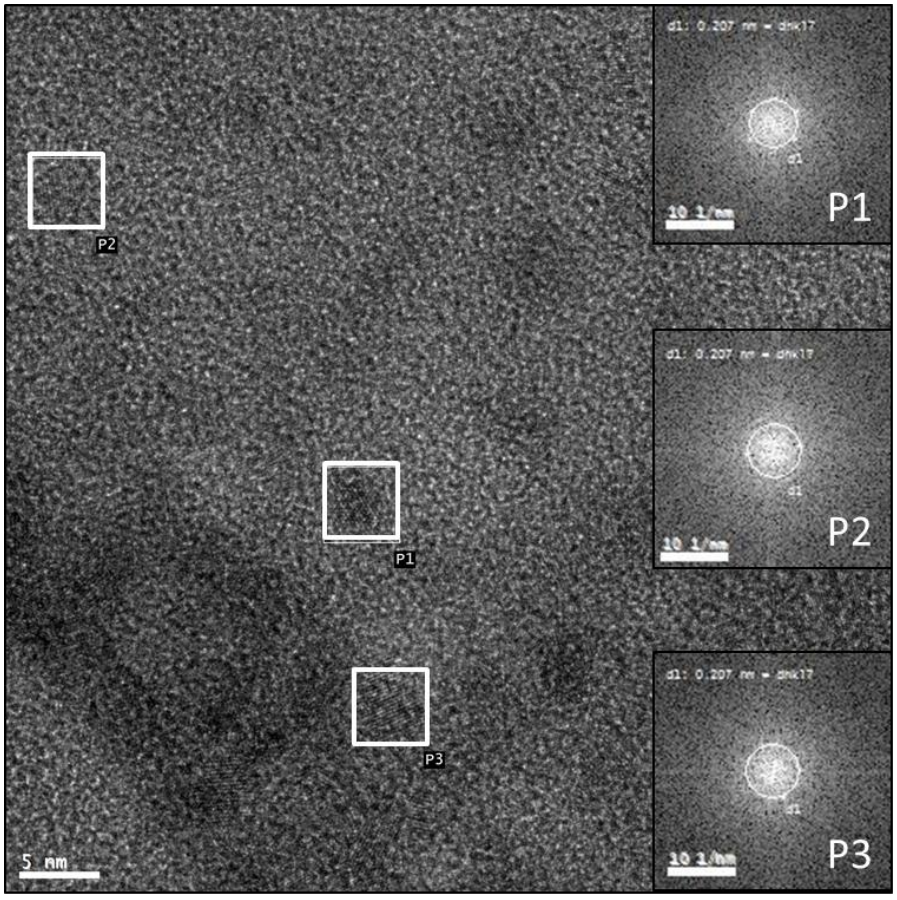

Figure 4.5 FFT analysis of HRTEM images, outlined nanocrystals have their FFT image in insets on the right

Cu contamination of the carbon coated grids may be a possible explanation for the observed lattice spacings, because they match with those of face centered cubic (FCC) Cu. Some particles even exhibited crystal twinning, which is common to metallic nanocrystals, but never mentioned for nc-Si. Several different types of TEM grids were used through the course of this work and all revealed the same type of particles, which indicates that the nanocrystals were probably not from contaminated grids. Cu dissolution and reduction may also have been the cause of the observation since it is possible for Cu to dissolve in nitric acid[79], but this would not explain the fluorescence and absorption characteristics that these solutions exhibited before observing them under TEM. Systematic experimentation to determine if the Cu grid was the source of the nanocrystals was not carried out due to the lack of other grid materials, such as Au or Ni to make comparisons.

Si is known to exist in at least 12 different high pressure polymorphs[80], making it possible that the nanocrystals viewed under TEM may be in one such phase. For example, at pressures above 8 GPa, diamond cubic Si can transform into a hexagonal phase with lattice spacings similar to those observed. These types of pressures may be possible during the sonication process, but this crystalline phase has not previously been reported in nc-Si produced using similar methods[39]. Although the observed spacings were similar to that of hexagonal phase silicon, they were not within experimental and calibration errors. As of yet, no high pressure polymorph has been identified as an acceptable match for observed nanocrystals.

Another material that nanocrystals may be composed of is quartz SiO_2. Trigonal α-SiO_2 has lattice spacings which are very similar to those observed under TEM. Lattice spacings of 2.1 Å and 1.8 Å were observed in nc-Si using a different synthesis process[34] and attributed to quartz SiO_2. These spacings were claimed to form during oxidation of their nc-Si. Lattice spacing of diamond cubic Si were observed in those nc-Si as well. The main issue with associating these nanocrystals with quartz is that this material has only been shown to form under hydrothermal and alkaline conditions[81]. Although hydrothermal pressures and temperatures may be present during the etching and sonication of the nanocrystals, the solutions are never alkaline.

Intensive TEM characterization of our nanocrystals was hampered by issues with sample preparation. Locating the particles was made difficult due to the small size of the crystallites and low concentrations. Imaging at high magnifications and STEM mode caused residual solvent molecules to crack and deposit over the area of the beam, burying the particles under a film of carbon.

4.4 Surface and Optical Properties of nc-Si

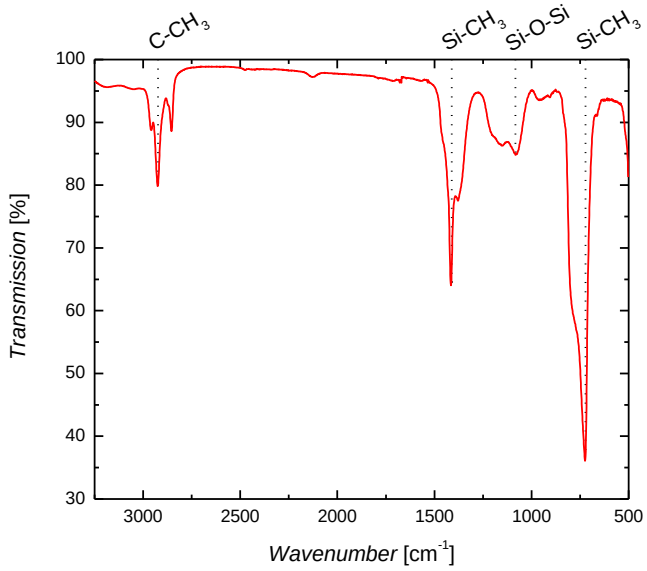

Figure 4.6 FT-IR transmission spectrum of nc-Si dispersed in NaCl

FT-IR spectrums of nc-Si samples were taken using the methods described in chapter 4. The transmission spectrum, represented by **Figure 4.6**, indicates four major absorption bands which are located between 720-790 cm^{-1}, 1050-1180 cm^{-1}, 1370-1420 cm^{-1}, and 2840-2970 cm^{-1}.

Table 4.2 provides the assignments for these bands as well as two other minor peaks found in the spectrum. This data indicates that the nc-Si are passivated by both oxides as well as some type of organic ligand. These organic ligands may have formed during the sonication process while the p-Si substrates were submerged in isopropyl alcohol. The nc-Si also shows a very weak absorption band associated with hydride termination, which would have been present on the p-Si surface after etching.

Table 4.2 Associated species for given peak positions found in nc-Si (obtained from ref [82] and [83])

Peak Position (cm^{-1})	Chemical Species	Mode
723-790	Si-CH_3	rocking or wagging
660	Si-H and Si-H_2	wagging-bending
893	SiH_2	scissor
945	SiH	bending (Si_2-H-SiH)
977	SiH	bending (Si_2-H-SiH)
1080-1160	Si-O-Si	asymmetric stretching
1375	C-H	deformation or bending
1417	C-CH_3 or Si-CH_3	deformation or Si-CH_2 scissor
2101	SiH	stretching
2853	C-CH_3 or Si-CH_3 terminal -CH_3 group	asymmetrical stretching
2924	C-CH_2	asymmetrical stretching
2961	C-CH_3 or Si-CH_3 terminal -CH_3 group	asymmetrical stretching

The nc-Si characterized by FT-IR and TEM exhibited UV-blue emission when excited by a 350 nm wavelength. After sonicating the p-Si substrates, the suspensions consisted of a wide range of sizes. Some of the larger aggregates were even visible to the naked eye. The PL spectrum, as shown in **Figure 4.7**, exhibited an emission peak at 656 nm before size separation procedures and 436 nm afterwards. The main method to separate sizes in these solutions was through centrifugation, which turned the suspensions from a cloudy solutions to a clear ones. This change in PL emission indicates that the larger aggregates emitted red, whereas the smaller particles emitted blue wavelengths.

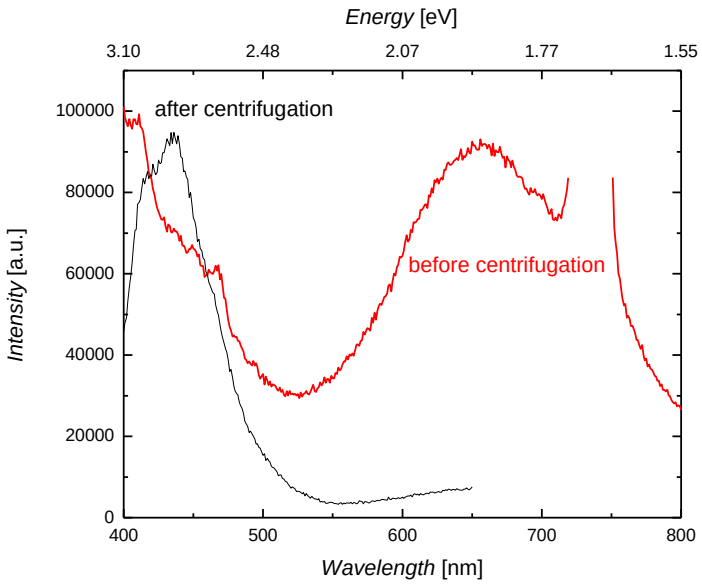

Figure 4.7 PL emission spectrum of nc-Si before and after centrifugation

Figure 4.8A shows the absorbance, PL excitation, and PL emission spectrums of nc-Si. The absorbance spectrum has a shoulder at around 280 nm which is similar to that of nc-Si particles prepared using a different synthesis approach[36]. The peak excitation is at 375 nm while the peak emission is 436 nm. The emission spectrum contained two emission peaks located at 412 nm and 436 nm. These peaks did not shift in relative intensity when excited at different wavelength, indicating that they are not caused by different populations of nanocrystal sizes. They are likely due to interactions of the excitons created in the nanocrystal and the surface groups, such as the oxides or alkyls found on the surface. **Figure 4.8**B illustrates how the two emission peaks could arise from separate surface states. Blue emission had been observed in nc-Si previously and had been attributed to oxygen related surface states[84].

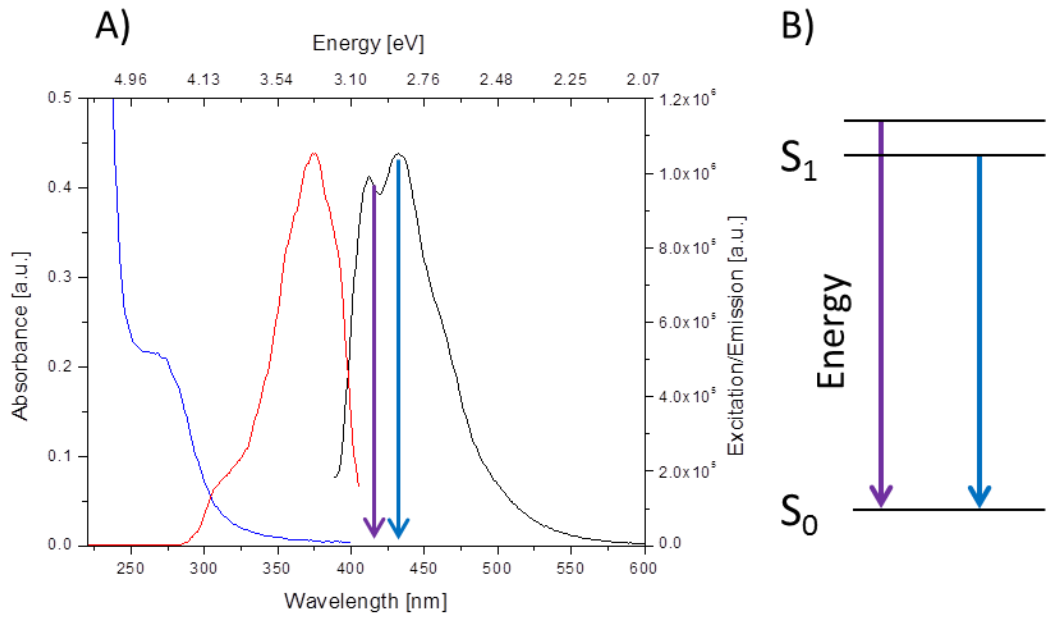

Figure 4.8 A)UV-Vis Absorbance (blue), PL excitation (red), and PL emission (black) spectra of nc-Si dispersed in IPA B) Simplified Jablonksi diagram of proposed energy transitions in nc-Si

Not all samples showed fluorescence after synthesis. Some samples had weak signals at their characteristic emission wavelengths, as demonstrated in **Figure 4.9**. However, after reconstituting the samples in the same solvent and volume, the fluorescence signal increased by at least two orders of magnitude. Reconstitution consisted of completely drying the sample under vacuum, adding back a solvent, and re-dispersing the material via sonication. This signal enhancement may be due to interactions between the nanoparticles that amplify the signal from single nanocrystals. Such collective effects in nanoparticle clusters have been shown to enhance their fluorescence [85].

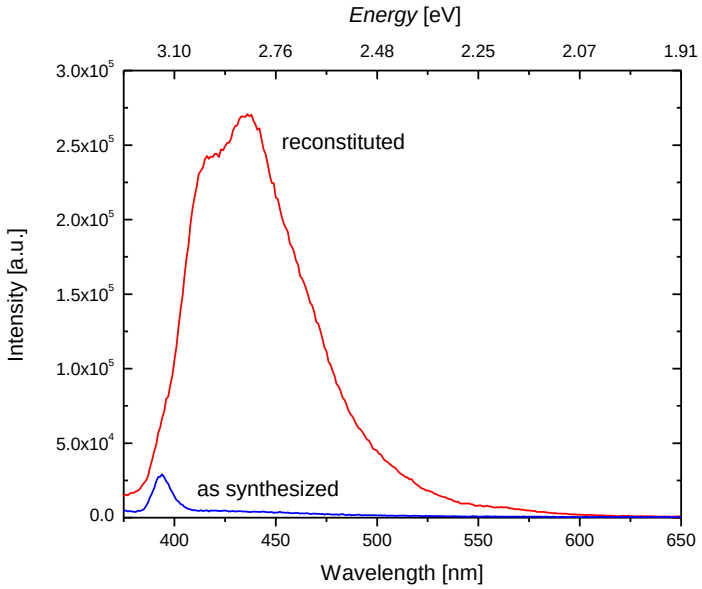

Figure 4.9 PL emission spectra of nc-Si dispersed in IPA before (blue) and after (red) reconstitution into the same solvent. The peak below 400 nm is due to the Raman signal of the solvent

Reconstituting samples in different solvents also had an effect on the emission intensity. Comparing tetrahydrofuran (THF), isopropyl alcohol (IPA), and acetonitrile (MeCN) containing the same concentration of nc-Si, it was found that ACTN showed the highest increase in emission (**Figure 4.10**). The interactions between nc-Si and the solvent have an effect on the emission, and this could be due to the polarity of the solvent as summarized in **Table 4.3**.

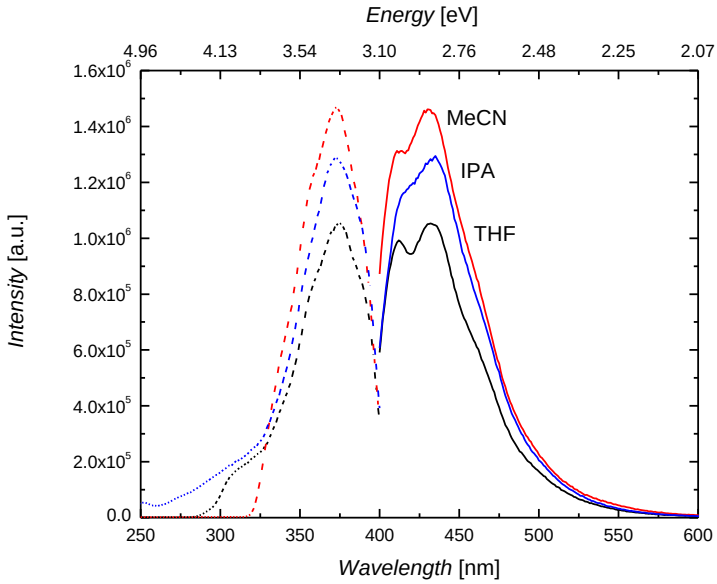

Figure 4.10 PL excitation (dashed) and PL emission of nc-Si reconstituted in THF(black), IPA(blue), and MeCN(red)

Table 4.3 Properties of THF, IPA, and MeCN with their respective peak emission intensities

Solvent	Type	Polarity(Dielectric Constant)	Emission intensity (counts/second)
THF	Polar Aprotic	21	1.461×10^6
IPA	Polar Protic	18	1.286×10^6
MeCN	Polar Aprotic	7.5	1.053×10^6

Yield calculations were determined through gravimetric analysis of the synthesized solutions. For an average synthesis we obtained approximately 45 µg/ml of solution. The amount of particles produced during each etching cycle per unit area of the substrate approaches ~3 µg/cm^2.

4.5 Summary

Sonication of stain etched Si using HF and HNO_3 yielded nanocrystals which exhibited UV-blue PL as well as other features which indicate that they may be composed of Si. However, due to the low synthesis yields and difficulty in obtaining

measurements, we were unable to determine a definitive composition. If these nanocrystallites were indeed a polymorph of crystalline Si, then they would be extremely interesting to the quantum dot community because only the diamond cubic phase of Si has ever been observed for nc-Si. If these particles are made of quartz, then understanding its formation and electronic properties would be of interest because quartz has never been studied at these dimensions. TEM measurements were the main source of characterization for this material due to their small size and low concentrations. This limited the amount of information that was available for analysis, making it difficult to form definitive conclusions. Even imaging these nanocrystals proved to be difficult. The effects of reconstituting the nc-Si particles were quite interesting, but understanding the effect requires further work. Much more work will need to be conducted on this synthesis technique to understand what type of material is being produced. In any case this was not an efficient method of creating nc-Si in large quantities.

In the next chapter we will present our work on stain etching using a different oxidant, $FeCl_3$.

5 RESULTS AND DISCUSSION: Stain Etching with $FeCl_3$ (ap-Si)

5.1 Introduction

In this chapter we will discuss the results of our efforts in synthesizing ap-Si suspensions. A wide array of characterization techniques were used to probe both the structural, chemical, and optical properties. The etching process yielded consistent results at higher concentrations, allowing for easier analysis of this novel material. Fluorescence spectrometry and FT-IR were the two main techniques used to study the relationship between these two properties. TEM, AFM, SEM, and Raman spectroscopy were used to investigate the structure and phase. XPS was used to determine the overall chemical composition of ap-Si. Porosimetry measurements were also taken to determine the porosity and surface area of the ap-Si particles. All of these characterization techniques taken together reveal the unique properties of ap-Si.

5.2 ap-Si Films

Stain etched films of ap-Si were created using $FeCl_3$ as the oxidizing agent and following the procedure outlined in chapter 4. Visibly, the stain etched ap-Si films displayed a dark orange yellow color when dried. As seen in **Figure 5.1**A&B, the etched films exhibited interesting features at the micron scale. The surface of the films is covered in nodules ~10 μm in diameter and ~5 μm in height with a gap between them and the bottom surface (**Figure 5.1**C). The nodules compose the top layer of the surface while the bottom layer consists of a film that seemed to be more adherent to the substrate. As revealed in **Figure 5.1**D, the nodules surfaces

consisted of porous features that were not resolvable at the resolutions we obtained using SEM.

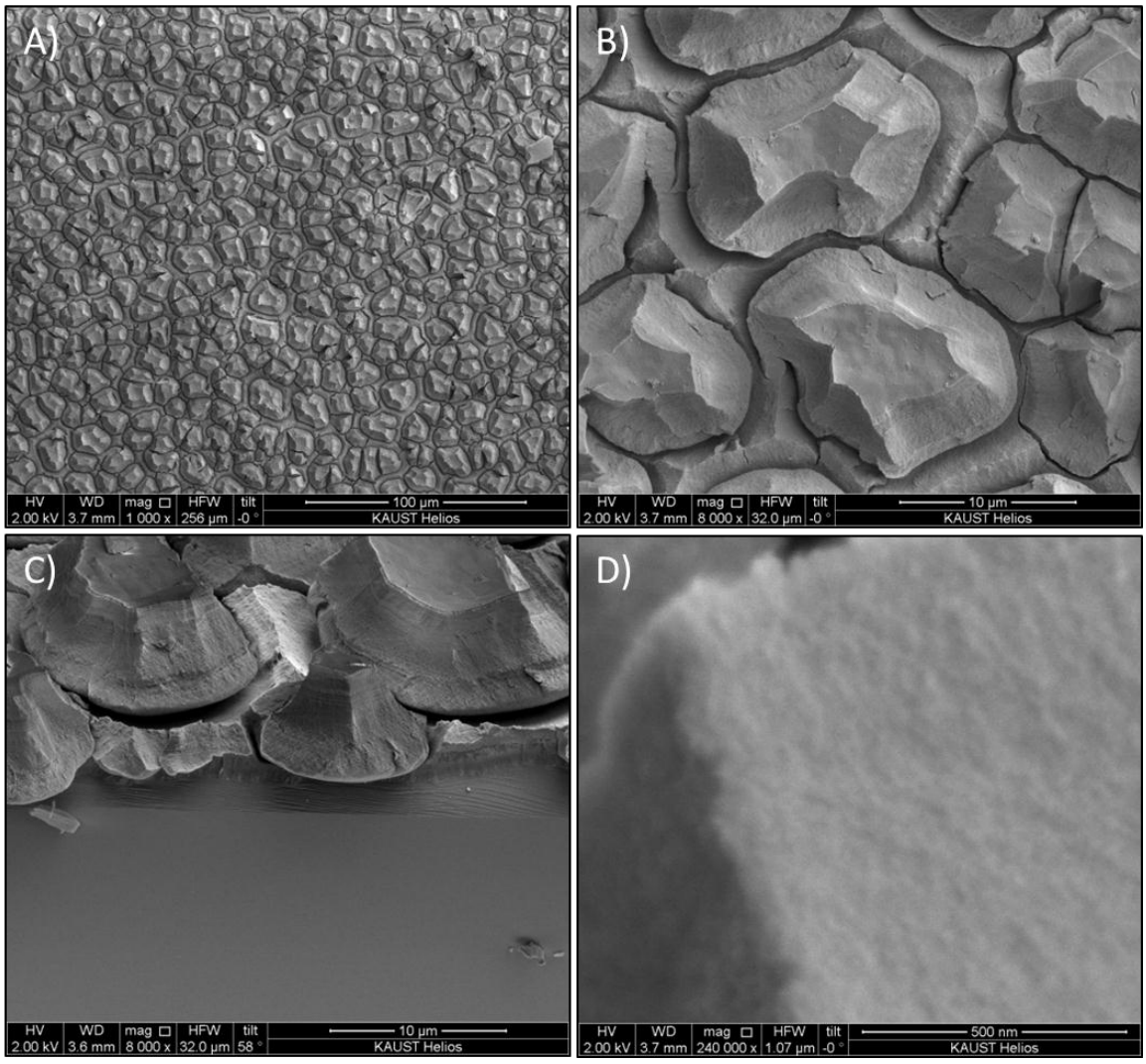

Figure 5.1 SEM micrographs of an $FeCl_3$ etched Si substrate before sonication A) and B) are top views of the surface while C) shows the cross sectional view and D) is a high magnification image of one nodule

The stain etched ap-Si films were sonicated in a solvent using a bath sonicator in order to remove the top layer of nodules from the Si substrate. After this sonication step, the solvent contained fine yellow particles of ap-Si whereas the etched substrates were matte black. SEM imaging of this sonicated film revealed that the

nodules were attached to the surface by circular stems, as displayed in **Figure 5.2**A&B. From **Figure 5.2**C, we can see that the bottom layer was measured to be ~2 μm thick, composed of pseudo-polygonal ridges with circular stems at their centroids, and arranged in what seems to be a Voronoi tessellation. Like the nodules, the surface of this bottom layer was also composed of porous features, but at larger scales (**Figure 5.2**D). From gravimetric analysis it was estimated that approximately 16 μm of Si were dissolved from the surface of Si substrate during the etching process.

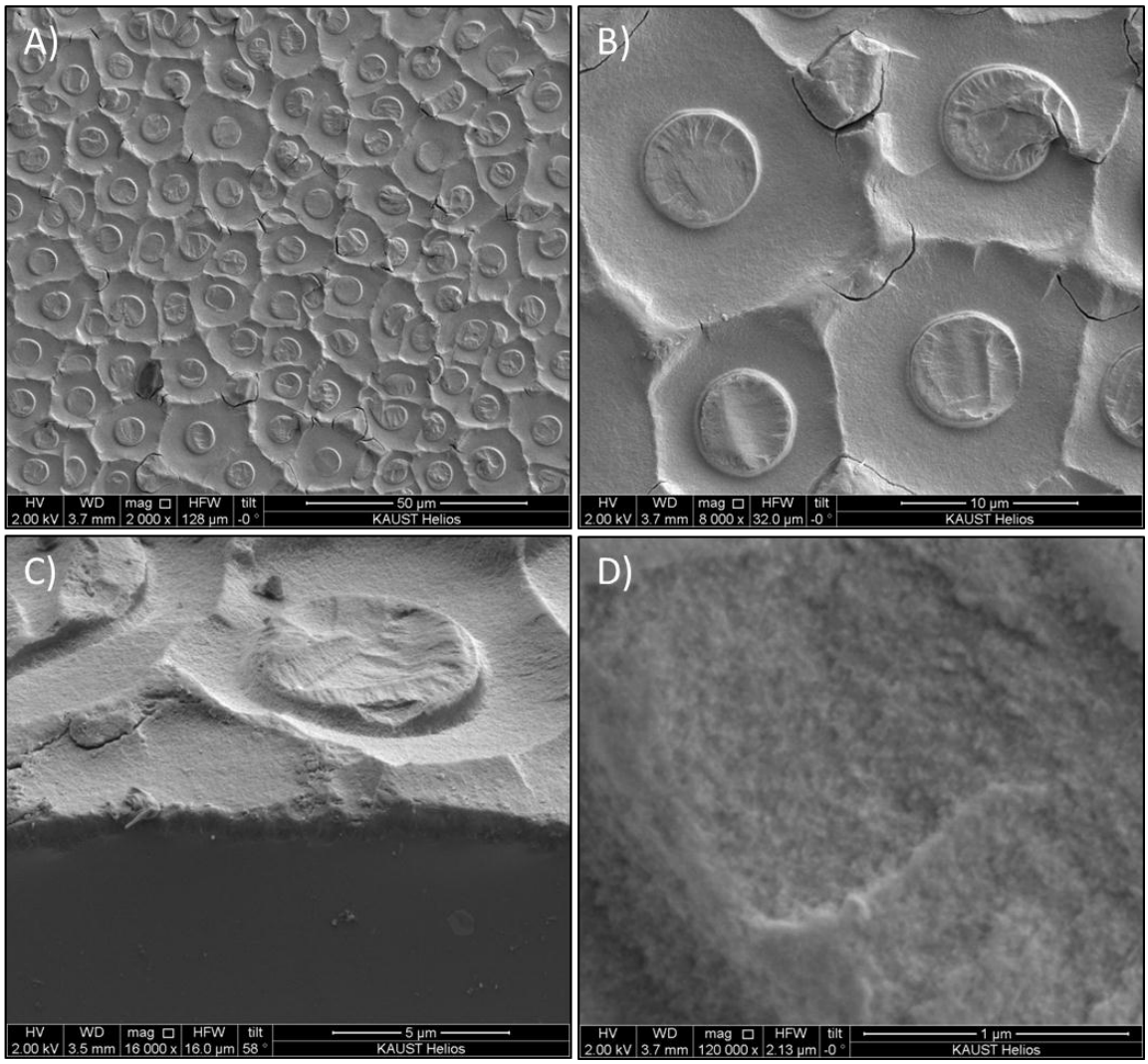

Figure 5.2 SEM micrographs of an $FeCl_3$ etched Si substrate after sonication A) and B) are top views of the surface while C) shows the cross sectional view and D) is a high magnification image of a circular feature

Both the as synthesized and sonicated surfaces displayed bright PL emission under UV excitation. However, both layers did not emit at the same wavelength. As shown in **Figure 5.3**, the etched film had an emission peak centered at 620 nm, whereas the sonicated films presented an emission peak at 638 nm. This shift in emission may be due to the difference in porosity of the top and bottom layers or as a result of interactions between the p-Si layers and the bulk Si underneeth. The films we

produced used conditions similar to those employed by Dudley et al.[71], yet we did not observe the same morphological properties. Although, they produced dual layer films made of a weakly adherent top layer and a well adhered bottom one, their structures were composed of planer sheets. Both of our p-Si films displayed different PL emission wavelengths before and after removing the top layer.

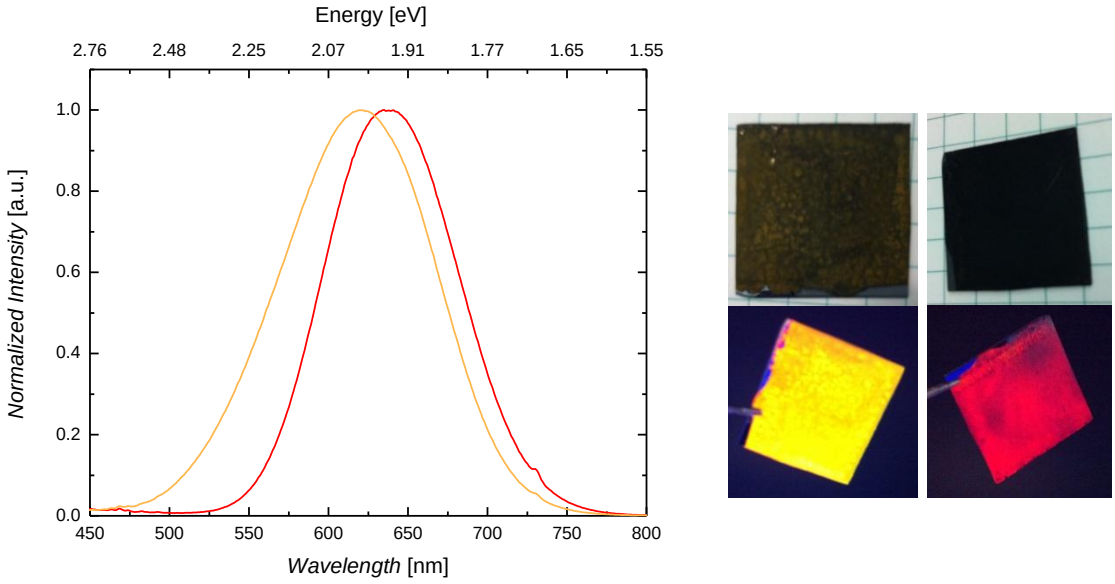

Figure 5.3 PL emission spectrum and images of ap-Si film before (orange 620nm) and after (red 638nm) sonication

5.3 ap-Si Particles

The bulk of our characterization work was conducted on ap-Si particle suspensions extracted from stain etched films. Creating suspensions allows for easier control of surface properties and size. It also has the added benefit of being able to be deposited as films on substrates other than Si, rendering an easier integration into devices or other applications. As displayed in **Figure 5.4**A, the bath sonicator removed the ap-Si nodules from the surface layer and created particles on the order of 10 μm in diameter. A higher magnification image of one particle shows the

location where a circular stem from the bottom layer attached to the particle, as well as concentric rings where the stem was being etched (**Figure 5.4**B). A probe sonicator was employed to further mill the particles in order to create colloidal suspensions that were analyzed for their fluorescence and absorbance properties. As seen in **Figure 5.4**C&D, this sonication step was successful in milling the ap-Si particles into the nanoscale.

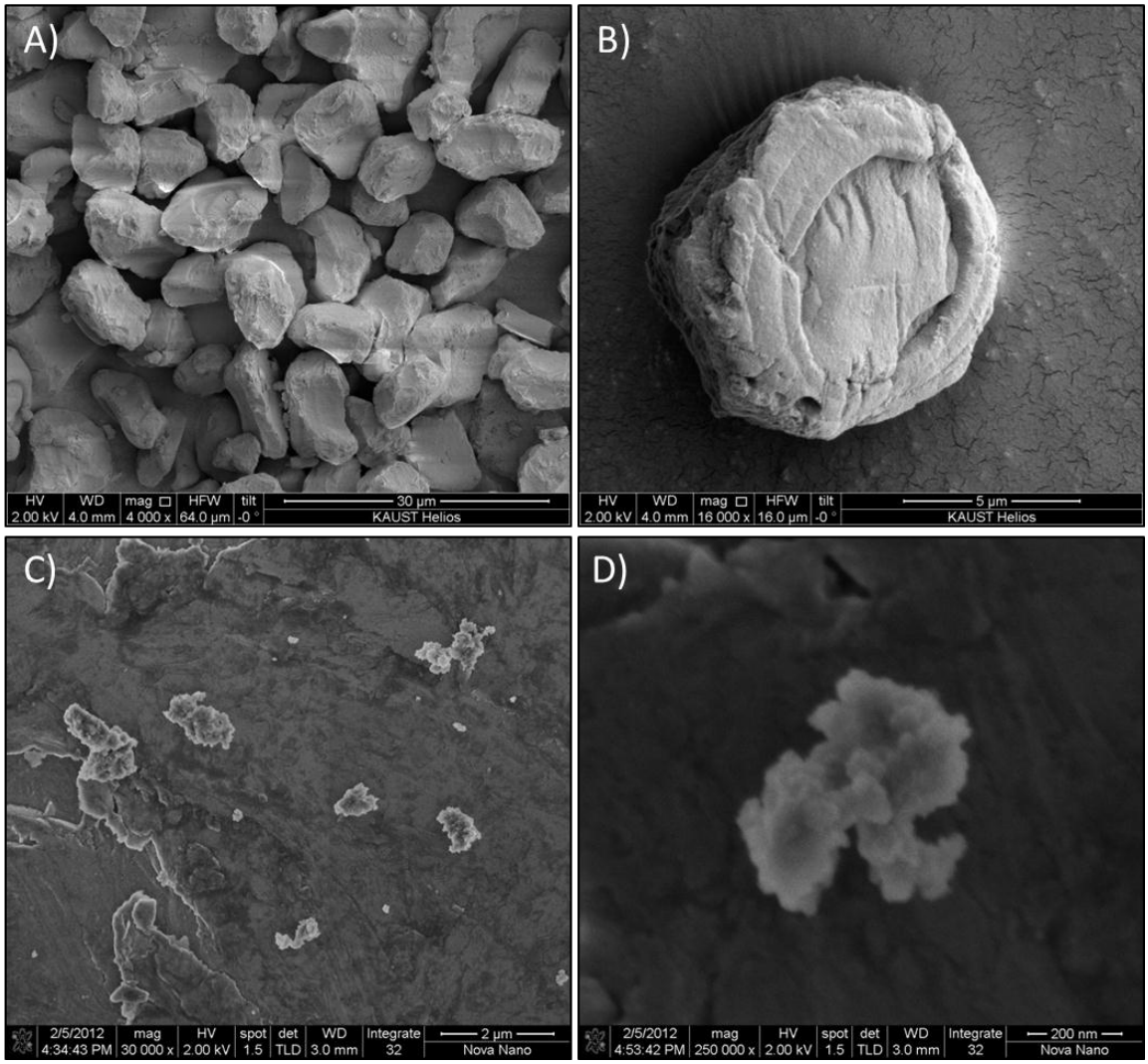

Figure 5.4 SEM micrographs of ap-Si particles A) nodules collected from the etched surface B) bottom side of one nodule C) ap-Si particles after ultrasonication D) is a high magnifaction image of one particle

The dimensions of these colloidal particles varied greatly, the smallest being on the order of hundreds of nanometers, whereas the largest were about two to three microns. Although lengths and widths were easily determined by SEM analysis, measuring heights were not as easy. AFM measurements were employed to help determine the size and shape of the ap-Si particles. As seen in **Figure 5.5**A&B, the topographical images were taken using AFM, showing that the heights also varied in a similar fashion as the other dimensions (**Figure 5.5**D). These results assume that there were only single particles that have been measured, and not stacked ones. Gravimetric analysis of the synthesized ap-Si revealed that the average yield was approximately 0.4 mg/cm^2 of etched surface. This was more than two orders of magnitude greater yield than what was obtained with nc-Si synthesis procedures. From yield measurements and the SEM images, it was estimated that the particles had approximately 60% porosity.

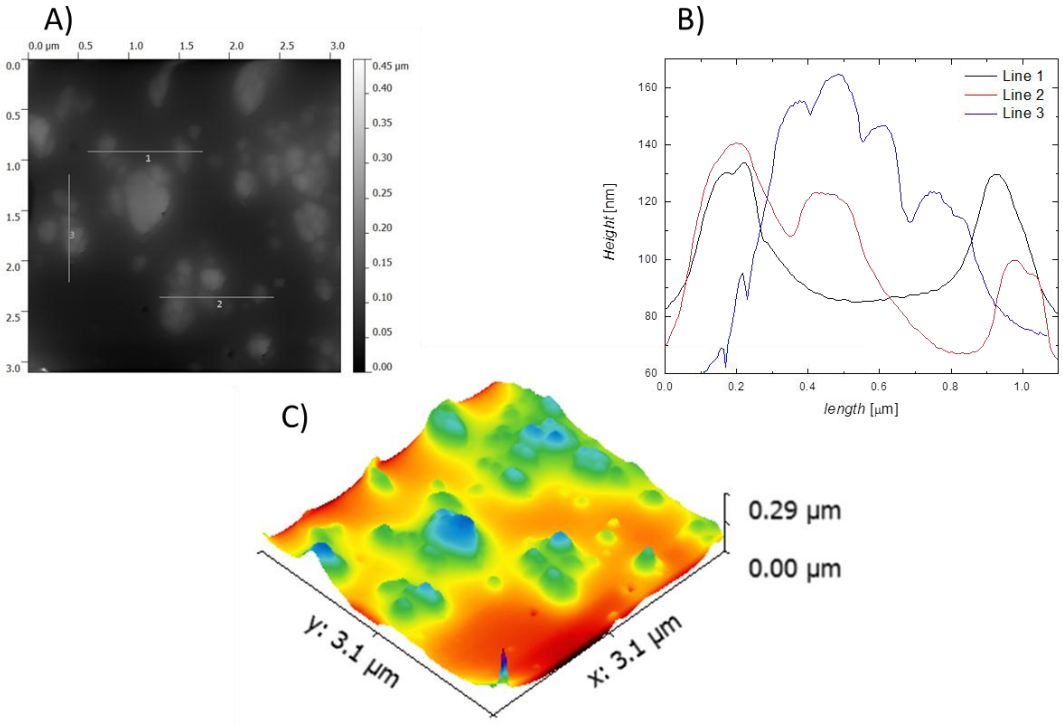

Figure 5.5 AFM topographical image of ap-Si particles after ultrasonication A) 2D view of surface B) corresponding lin scans C) 3D rendering of surface

TEM imaging on ap-Si particles revealed a highly porous structure, composed of a lacey network of nanometer scale bridges which connect larger aggregates of material (**Figure 5.6**A). Higher magnifications in **Figure 5.6**B show that these bridges vary in scale between 2-10 nm, connecting multilayer aggregates. The diffuse character of the SAED of this material revealed only an amorphous phase (inset **Figure 5.6**B). p-Si films created by using similar etchant compositions and Si substrates have been claimed to be composed of nanocrystalline Si [70]. This complete change of phase between the initial crystalline Si substrate into an amorphous porous film has previously been observed in anodic and stain etched Si. These observed phases have been attributed to a spontaneous crystalline to amorphous phase transition, which is initiated once the Si crystallites shrink below

some critical value during the etching process[86]. Pressure induced amorphization[87] may have also caused this phase transition to occur. At pressures above 7 GPa, porous crystalline silicon has been observed to change to an amorphous phase. The high surface area along with possibly trapped hydrogen gas may have provided the pressure needed for a phase transformation to occur.

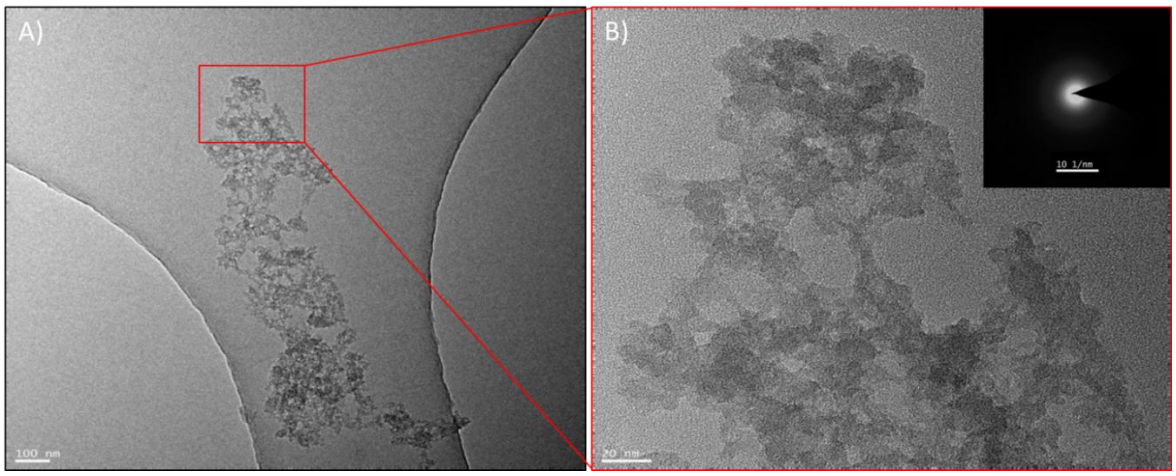

Figure 5.6 A) TEM image of an ap-Si particle B) higher magnification image, SAED pattern is shown in the inset

As presented in **Figure 5.7**, the ap-Si we synthesized was composed of particles that contained features at various dimensions, including pores and nanowire bridges (**Figure 5.7**A). EDS analysis revealed Si and O as the major elemental constituents in this material with Cu and C signals emitted from the TEM grid (**Figure 5.7**B).

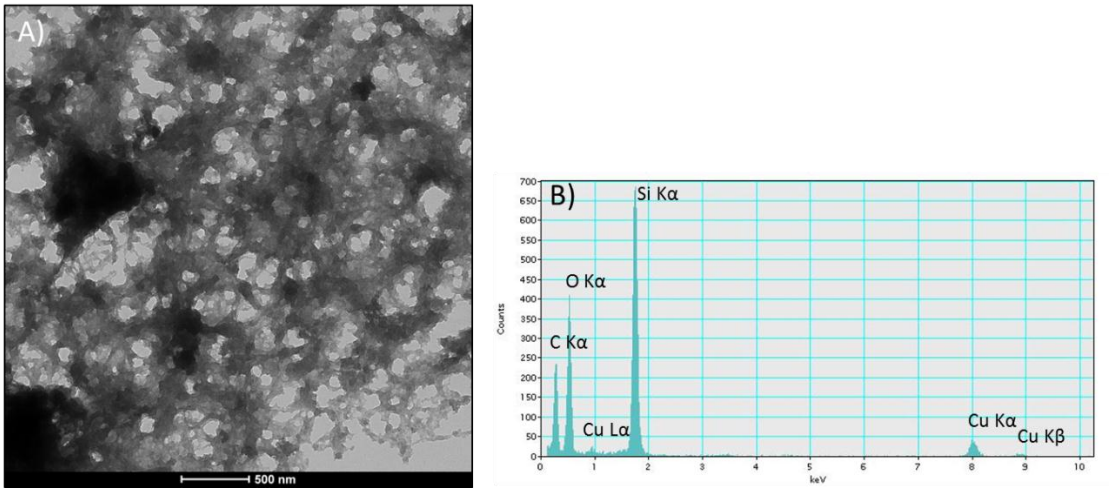

Figure 5.7 A) TEM image of ap-Si B) corresponding EDS spectrum

In order to quantitatively determine the surface area of our ap-Si, we conducted BET analysis of nitrogen adsorption-desorption isotherms shown in **Figure 5.8**. The response of the ap-Si particles corresponds to a type II adsorption isotherm. The hysteresis loop observed in these isotherms is a result of capillary condensation of the N_2 gas into the meso/micropores of the ap-Si. A surface area of ~493 m^2/g and an average pore diameter of ~3.2 nm were calculated from these curves.

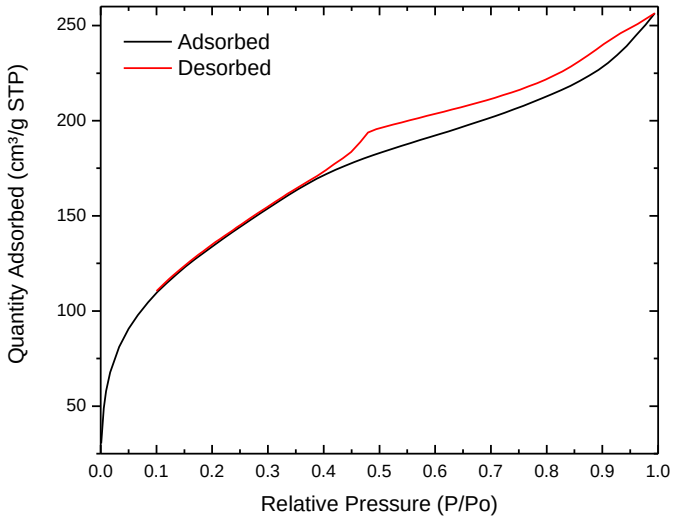

Figure 5.8 Nitrogen adsorption-desorption isotherms at 77 K for ap-Si

Figure 5.9 shows the Raman spectrum of ap-Si, the two main features that can be observed are peaks at 480 cm^{-1} with a tail extending below 450 cm^{-1} and a peak at 150 cm^{-1}. These features are characteristic of amorphous silicon[88] with 480 cm^{-1} and 150 cm^{-1} representing the transverse optical (TO) and transverse acoustic (TA) bands respectively. The 150 cm^{-1} peak is not found in the crystalline phase because translational invariance leads to k selection rules which forbid light scattering by phonons in this spectral region. This type of peak is traditionally called the boson peak, but in a-Si the boson and TA mode overlap[89]. The shoulder located below the 480 cm^{-1} is accounted for by the longitudinal acoustic (LA), 300 cm^{-1}, and longitudinal optical (LO), 380 cm^{-1}, of a-Si[90].

Using the TO and TA modes, it is possible to measure the degree of disorder in solids. Both the intermediate range disorder and bond angle disorder can be

estimated using these Raman spectra. The intermediate range disorder can be estimated using the intensity ratio between the TA and TO (TA/TO) bands. The root mean square, rms, bond angle disorder, Δθ, can be determined by the width of the TO band (Γ_{TO}) and the equation 7 [91].

$$\Gamma_{TO} = 15 + 6\Delta\theta \qquad (7)$$

The calculated values for these two terms are given in Table **5.1**. The difference in the TA/TO ratio and Δθ indicates that laser irradiation is increasing the degree of disorder in the structure.

Table 5.1 TA/TO, $\Gamma_{TO,}$ and Δθ of ap-Si vs. laser irradiation

Scan	Inter. Range Disorder (TA/TO)	TO Band Width Γ_{TO}	Bond Angle Disorder (Δθ)
1	0.78	96.4 cm^{-1}	13.6°
2	0.85	105.2 cm^{-1}	15°

Photobleaching can be seen as a decrease in the intensity of the spectrum at Raman shifts greater than 700 cm^{-1} with continued exposure to the laser. Si-O bonding vibrations (800-1100 cm^{-1}) also become visible as a result. The weak signal from Si-H and Si-H_2 wagging vibrations are also visible at 640 cm^{-1} [92] which further decreases intensity with increasing exposure to the excitation laser. These effects created by the excitation laser may be due to the removal of surface bonded hydrogen and/or oxygen, creating non-radiative dangling bonds that also increase the degree of disorder.

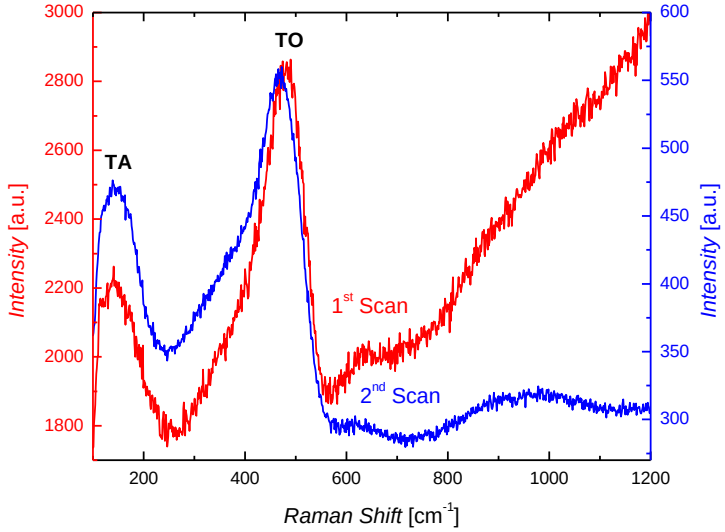

Figure 5.9 Raman spectra of ap-Si showing an initial scan and a second scan on the same location

As presented in **Figure 5.10**A, XPS elemental analysis revealed that the surface contained mainly Si and O with only trace amounts of F detectable and likely originating from residual Si-F bonds that were formed during the etching process. C was also detected and most probably a result of residual solvent molecules that remained on the surface after sample preparation. Elemental hydrogen was not detectable due to the limitations of this technique. Nevertheless this wide scan spectrum shows that no residual materials from the etching process were left on the ap-Si. A valence band spectrum was also taken in order to verify the existence of an amorphous Si structure (**Figure 5.10**B). Crystalline Si typically consists of three peaks located at 3, 7.5, and 10 eV. Due to the presence of over coordinated Si, the peaks near 7.5 and 10 eV merge to become a single broad peak [93]. For our ap-Si

the spectrum consists of broad peak between 15 and 5 eV as well as a shoulder around 3 eV, further confirming the presence of an amorphous phase.

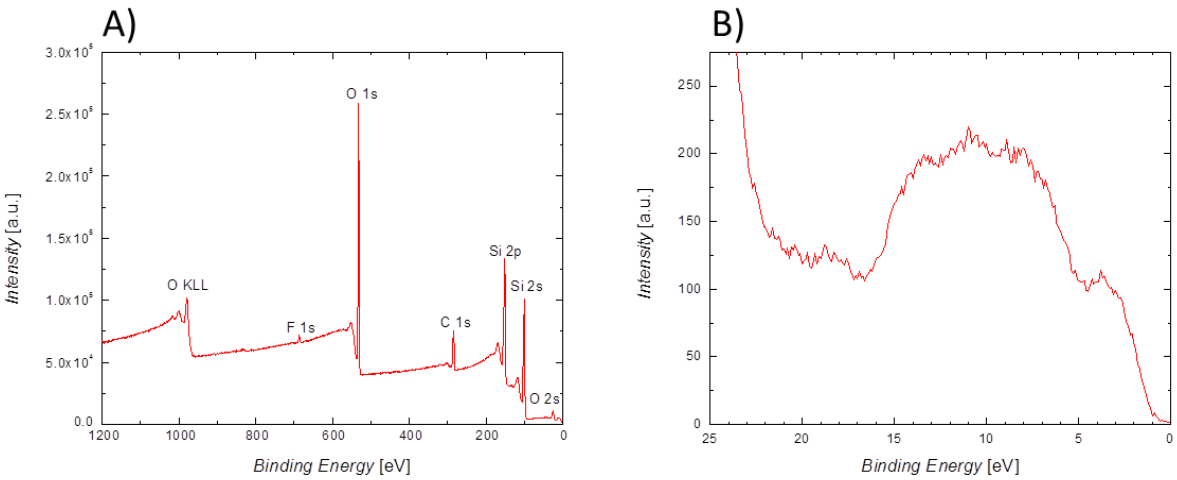

Figure 5.10 A) XPS wide scan spectrum of ap-Si B) XPS valence band spectrum

Further analysis of the Si 2p region of the spectrum, displayed in **Figure 5.11**, showed that the surface contained Si at various states of oxidation.

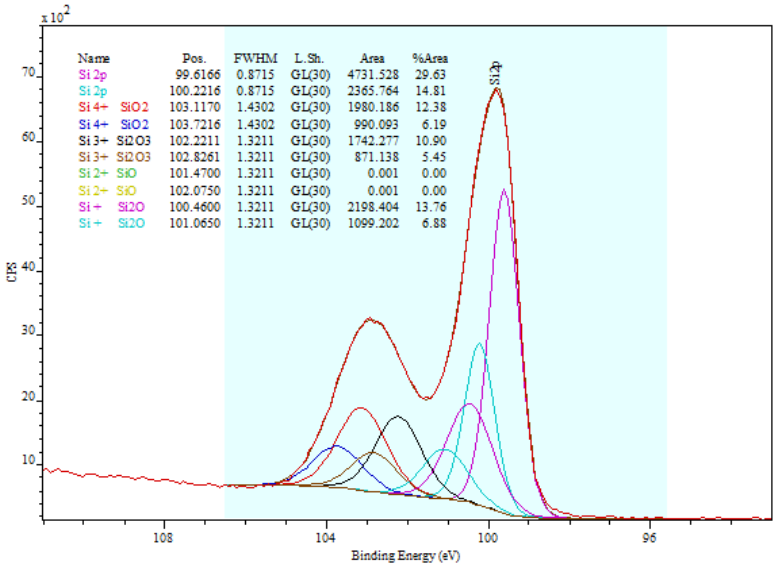

Figure 5.11 Deconvoluted Si 2p core level spectrum of ap-Si (the Si 2p XPS peaks analyzed by means of a Gaussian peak)

The atomic concentrations of the major elements detected through XPS are sumerized in **Table 5.2**.

Table 5.2 Concentrations of O, C, and Si calculated from XPS

Elements	O	C	Si
Atomic Concentration (%)	30.1	16.6	53.3

5.4 Optical and Surface Properties of ap-Si

The ap-Si particles extracted from stain etched films exhibited bright orange-yellow photoluminescent emission directly after synthesis. However, depending on the solvent this emission did not stay constant; it changed in both intensity and wavelength with time. Several factors were found to be responsible for this behavior. Presented in **Figure 5.12** is the 3D excitation vs. emission spectrum of one sample of ap-Si dispersed in toluene (**Figure 5.12**a) that exhibited a peak emission at 607 nm, and a peak excitation at 346 nm. The feature located behind the peak is an artifact of the data collection and is seen in the 2D map as a diagonal streak (**Figure 5.12**b). It represents the second order emission by the excitation source. What is unique about these results is that all the particles in the suspension, regardless of the size, produce homogenous emission. It was noted that after ultra-sonication using the sonicating probe, the toluene itself exhibited blue emission (see appendix 8.2).

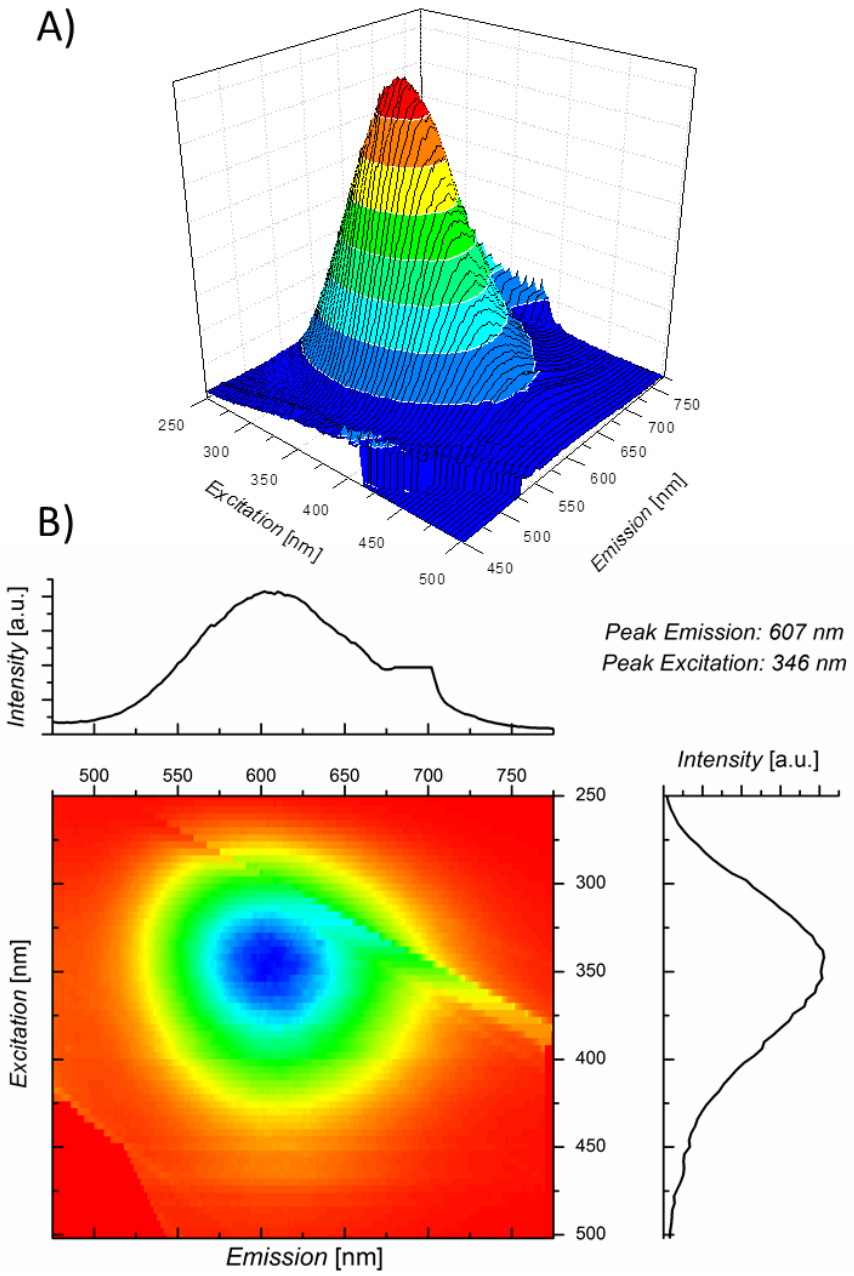

Figure 5.12 A) 3D rendering of PL excitation vs. emission B) 2D view indicating peak excitation and emission spectra for ap-Si

Shown in **Figure 5.13** is a typical UV-visible absorbance spectrum of ap-Si suspensions. It reveals that this material absorbs strongly at wavelengths below 400 nm. After synthesis these suspensions displayed a yellow or orange color under

white light. This can be attributed to a weak absorption tail from 400 nm onwards. The properties of this spectrum are similar to those reported for colloidal silicon solutions[94].

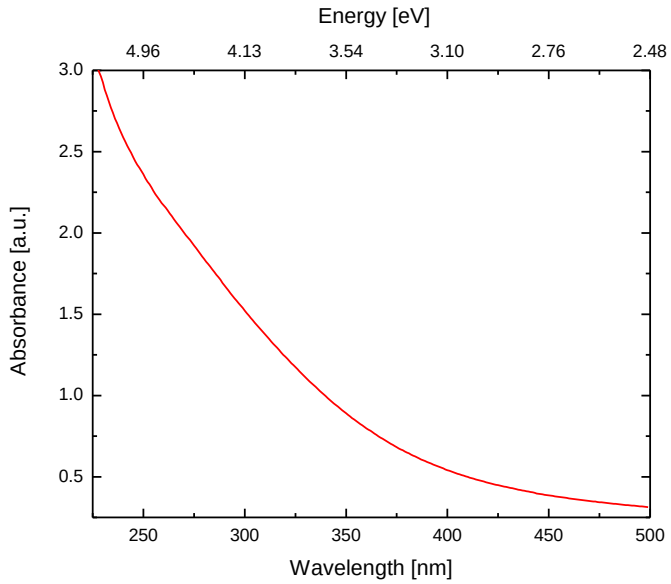

Figure 5.13 Absorbance spectrum of ap-Si dispersed in ethanol

Preliminary fluorescence lifetime measurements were conducted on two ap-Si suspensions dispersed in ethanol, displayed in **Figure 5.14**. One issue that was discovered was that the peak emission wavelength red shifted 70 nm compared with ones measured using the Horiba spectrofluorometer. Suspensions that showed visible dark orange emission under UV light and emission at 610 nm using the Fluoromax4 (Horiba), were measured to have a peak emission in the 680 nm on the F900 (Edinburgh Instruments). These differences may be attributed to miscalibration of fluorometer used to measure the lifetime. Nevertheless, when comparing two samples that have a difference in emission of 48 nm, they show

different average decay lifetimes. The higher energy emission had a lower lifetime; the results are summarized in **Table 5.3**. The multiexponential decay found on these suspensions may be a result of surface localized carriers. Multiexponential decay found in other light emitting semiconductor systems (CdSe quantum dots) have been attributed to these effects as well[95].

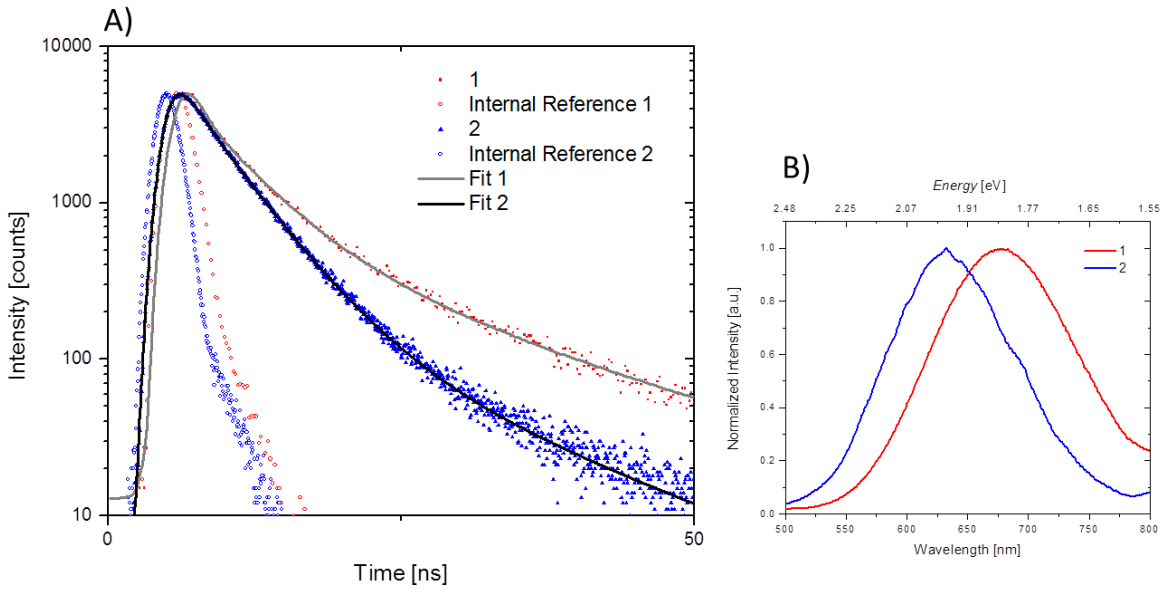

Figure 5.14 A) fit of the luminescence decay to three exponentials and the instrument response B) corresponding emission spectra of sample 1 and 2

Table 5.3 Summary of fit data corresponding to the curves in **Figure 5.14**

$$\textbf{Fit} = \mathbf{A} + \sum_{i=1}^{3} \boldsymbol{B_i e^{-\frac{t}{\tau_i}}}$$

Sample 1:	τ_1	0.56 ns	B_1	0.17
τ_{avg} = 6.85 ns	τ_2	4.40 ns	B_2	0.06
	τ_3	15.1 ns	B_3	0.01
Peak Emission: 680 nm	χ^2	1.4	A	12.9
Sample 2:	τ_1	1.46 ns	B_1	0.01
τ_{avg} = 4.99 ns	τ_2	4.11 ns	B_2	0.02
	τ_3	13.9 ns	B_3	0.001
Peak Emission: 632nm	χ^2	1.0	A	1

Figure 5.15 demonstrates how temperature effects PL emission in ap-Si. We measured PL emission at temperatures ranging from 60 °C (333 K) to -6 °C (267 K) and found a linear relationship between the two properties within this range. The peak emission wavelength did not change through the temperature range. This reveals that the probability for an exciton to thermalize radiatively increases at lower temperatures, as is the case with all fluorescent nano-scaled semiconductors. For bulk a-Si, PL measurements are usually take below 100 K with a maximum intensity obtained around 50 K and strong quenching occurring at temperatures above 100 K. In the bulk a-Si system, it is believed that as temperature increases more and more carriers are released from the band tail states into conductive states from which they can easily diffuse to defect centers and recombine non-radiatively[96]. This process may occur in ap-Si but at a much higher temperature due to spatial confinement effects. However, to have a full understanding of how temperature affects the PL properties of ap-Si a larger temperature range is needed in order.

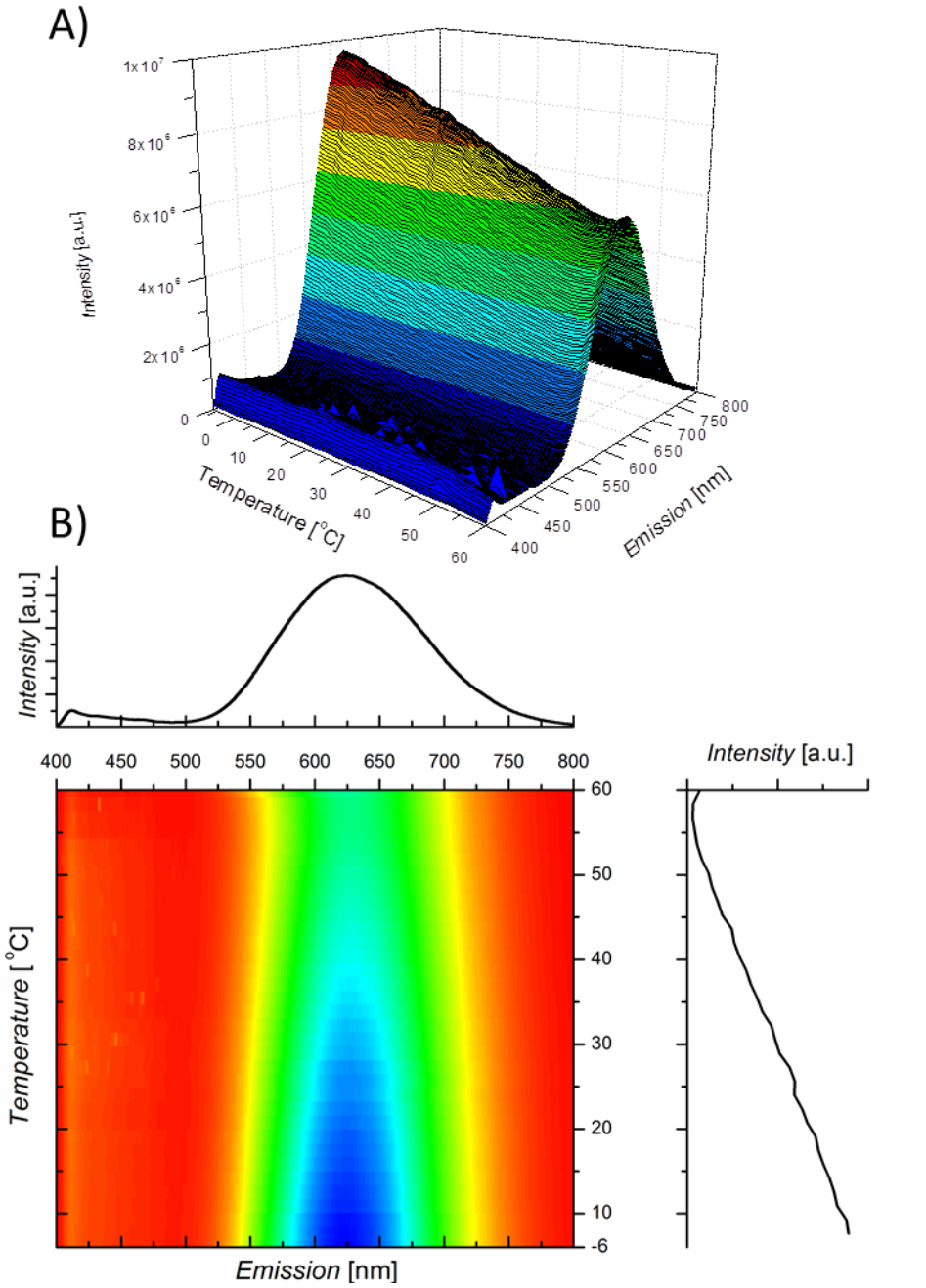

Figure 5.15 A) 3D temperature dependence of PL in ap-Si B) 2D view with peak emission and temperature vs. PL intensity

5.5 Oxidation Effects on ap-Si

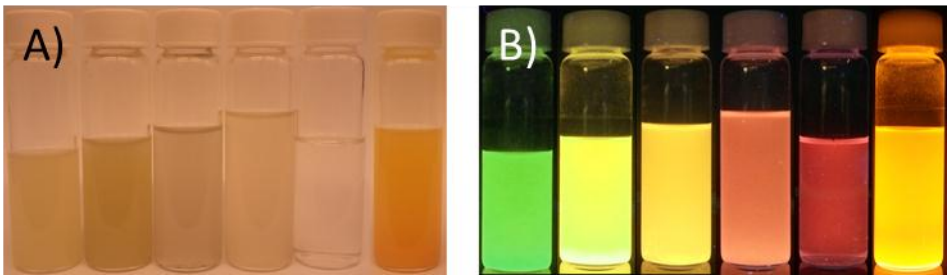

Figure 5.16 Images of ap-Si suspensions a) before UV illumination b) under UV 365nm illumination with a 450 nm cut off filter, the suspension on the far right of both images is dispersed in toluene, the rest are in ethanol

ap-Si particles, pictured in **Figure 5.16**, were found to be very sensitive to oxygen exposure. Although precautions were taken to limit the amount of dissolved gasses in the solvent and to keep the solutions under an inert N_2 atmosphere, ap-Si suspensions exhibited signs of oxidation. **Figure 5.17** presents the various wavelengths observed for ap-Si. Initially, suspensions synthesized in ethanol emitted an orange color, which over time ranged between green/yellow (520 nm) up to dark orange/red (620 nm) color. Samples synthesized in toluene, however, showed much more stable emission characteristics. The emission spectrum for all wavelengths was uniform with a FWHM of around 100 nm.

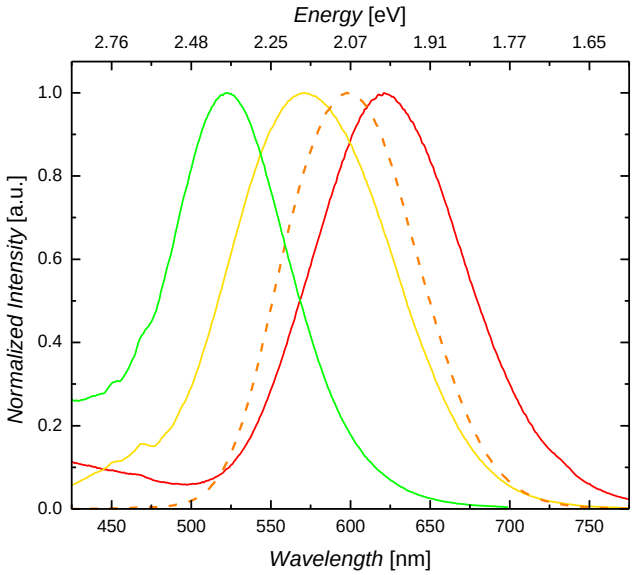

Figure 5.17 PL emission spectra of ap-Si in toluene (dashed) and ethanol (solid) samples

FT-IR absorbance spectra, displayed in **Figure 5.18**, showed a strong correlation between the relative concentration of different surface species and the PL emission wavelength. Surface hydrides, represented by absorbance bands around 670 cm^{-1}, 860 cm^{-1}, 903 cm^{-1}, and 2100cm^{-1} are present in ap-Si that exhibit emission wavelengths less than 600 nm. The width of the band centered at 2100 cm^{-1} indicates that Si-H, Si-H_2, and Si-H_3 groups are all present on the surface[97]. ap-Si dispersed in toluene contained both hydrides and oxides on the surface while emitting brightly at 610 nm. Oxidized hydrides represented by absorbance bands around 880 cm^{-1} and 2250 cm^{-1} were present for particles dispersed in ethanol. Their concentrations relative to the hydride species shift the emission wavelength of the suspensions. Surface oxides, represented by absorbance bands around 1070 cm^{-1} and 835 cm^{-1}, were present in all FT-IR measurements and are attributed to the

oxidation which occurs during the rinsing steps of the synthesis process as well as the presence of oxygen in the solvents. A summary of absorbance bands with their associated chemical species is presented in **Table 5.4**. A Schematic of the surface of ap-Si is shown in **Figure 5.19**.

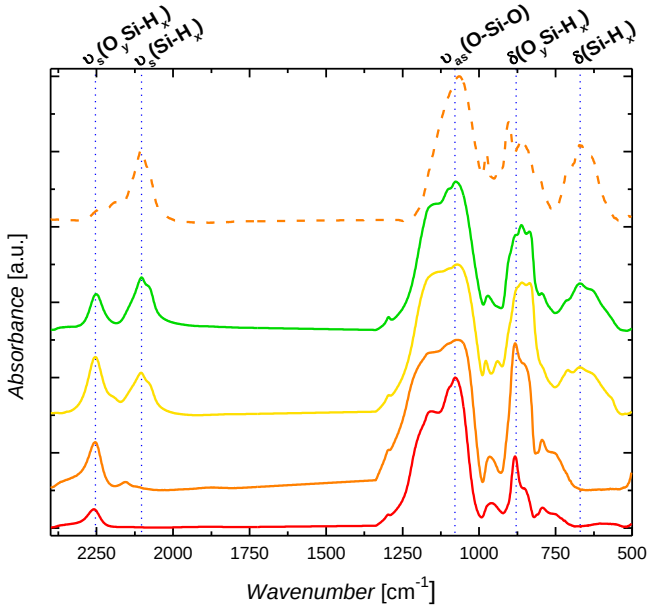

Figure 5.18 FT-IR absorbance spectra of ap-Si, colors correspond to those in Figure 5.17

Table 5.4 Assignments of absorbance bands in the FT-IR spectra of ap-Si from [98]

Band Position (cm^{-1})	**Chemical Species**	**Mode**
670	$\delta(Si\text{-}H_x)$	deformation
792	$\nu_b(SiO\text{-}H)$	bending
835	ν_b (O-Si-O)	bending
860	$w(Si\text{-}H_2)$	wagging
880	$\delta(O_ySi\text{-}H_x)$	deformation
903	$\delta(Si\text{-}H_2)$	deformation
1070/1150	ν_{as} (Si-O-Si)	asymmetric stretching
2100	$\nu_s(Si\text{-}H_x)$	symmetric stretching
2250	$\nu_s(O_ySi\text{-}H_x)$	symmetric stretching

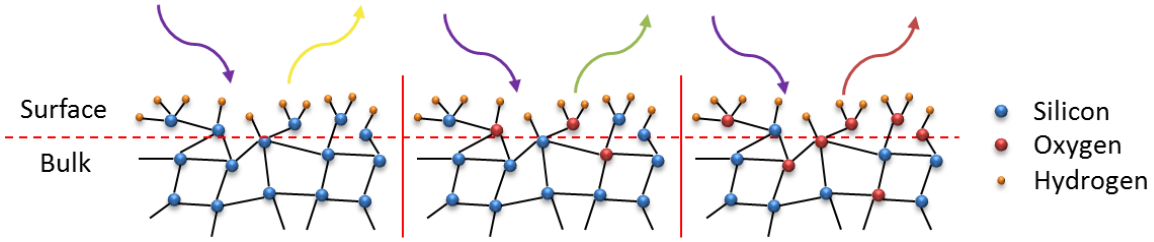

Figure 5.19 Schematic illustrations of surface species on ap-Si at different levels of oxidation

5.6 Controlled Oxidation of ap-Si

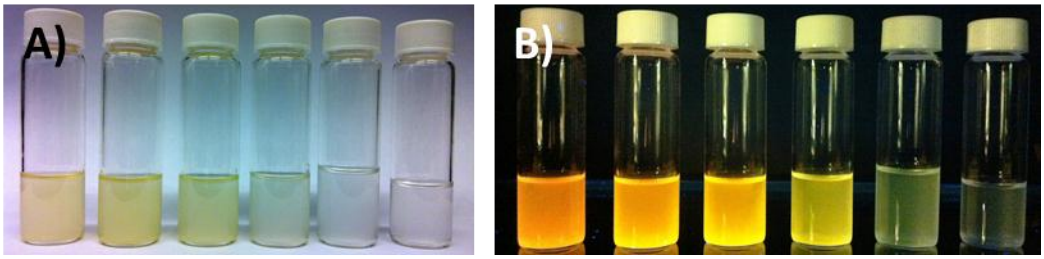

Figure 5.20 Images of achievable PL emission in ap-Si suspensions with H_2O_2 a) before UV illumination b) under UV 365nm illumination with a 450 nm cut off filter

In order to get a better understanding of this system, controlled oxidation of ap-Si was carried out under a N_2 atmosphere. Hydrogen peroxide was used as an oxidizing agent because it can decompose into two OH molecules[99]. These OH groups are highly reactive and can easily form silicon hydroxide bonds.

Figure 5.20 displays the range of emissions observed with ap-Si solutions containing various concentrations of H_2O_2. PL emissions ranged between 600 nm to 560 nm (**Figure 5.21**). The initial solution of ap-Si containing no peroxide showed yellow emission. The addition of peroxide first red shifted the emission reaching a limit around 600 nm before blue shifting down to 566 nm. 566 nm was the lowest wavelength emission achievable; increasing the peroxide concentration after this

limit only decreased the emission intensity. **Table 5.5** summarizes the conditions and results of the H_2O_2 experiments with the reference numbers corresponding to those found in **Figure 5.21**, **Figure 5.22**, and **Figure 5.24**.

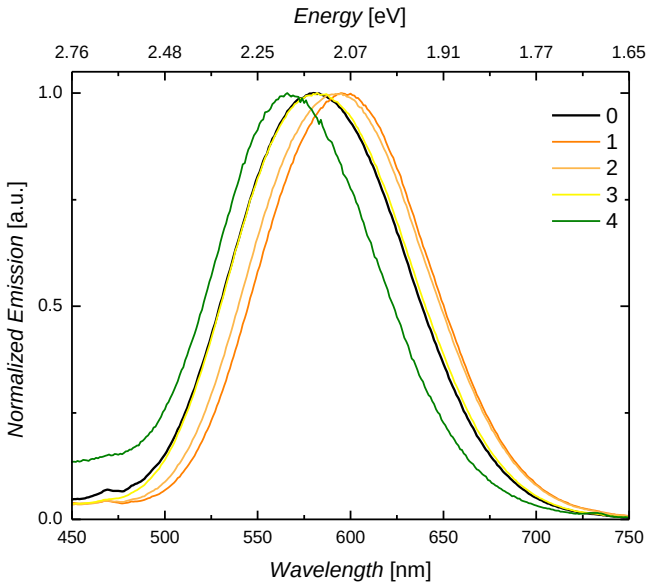

Figure 5.21 PL emission of ap-Si with increasing H_2O_2 concentrations

Table 5.5 Summary of results form H_2O_2 experiment

Ref	ap-Si (ml)	H_2O_2 (ml)	% H_2O_2	Peak (nm)	Δ (nm)	FWHM (nm)
0	5	0	0	580	0	108
1	5	.02	.398	595	+15	105
2	5	.06	1.186	589	+9	108
3	5	.18	3.475	582	+2	110
4	5	.72	12.587	566	-14	102

Analysis of the FT-IR spectra corresponding to the different experimental conditions demonstrates the relationship between emission energy and surface species (**Figure 5.22**). The untreated sample contained only oxidized hydrides and oxides on the surface. With the addition of H_2O_2, the concentration of surface hydrides

disappeared. This can be seen by the decrease in intensity of $\nu_s(O_ySi\text{-}H_x)$ and $\delta(O_ySi\text{-}H_x)$ vibration modes, located at 2250 cm^{-1} and 880 cm^{-1} respectively. Si-OH bond formation can be seen by the increased intensity of related absorbance bands, specifically those located at 3620 cm^{-1}, 940 cm^{-1}, and 792 cm^{-1}. **Table 5.6** summarizes all the major observable absorbance bands found in this experiment. **Figure 5.23** gives a schematic representation of the surface species found on ap-Si and its respective emission colors.

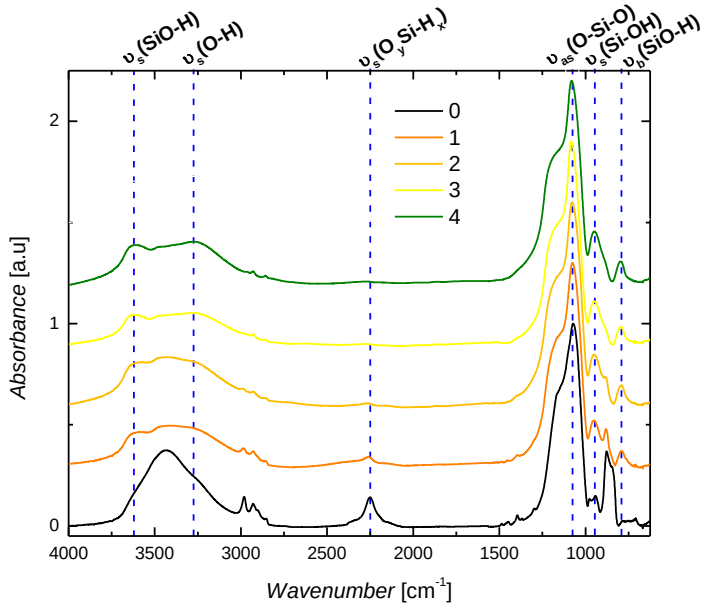

Figure 5.22 FT-IR absorbance spectra of ap-Si with increasing H_2O_2 concentrations

Table 5.6 Assignments of absorbance bands in the FT-IR spectra of ap-Si from Figure 5.22 [98], [99]

Band Position (cm^{-1})	Chemical Species	Mode
792	$\nu_b(SiO\text{-}H)$	bending
880	$\delta(O_ySi\text{-}H_x)$	deformation
940	$\delta(Si\text{-}OH)$	symmetric stretching
1070/1150	ν_{as} (Si-O-Si)	asymmetric stretching
2250	$\nu_s(O_ySi\text{-}H_x)$	symmetric stretching
3275	$\nu_s(O\text{-}H)$	symmetric stretching
3620	$\nu_s(SiO\text{-}H)$	symmetric stretching

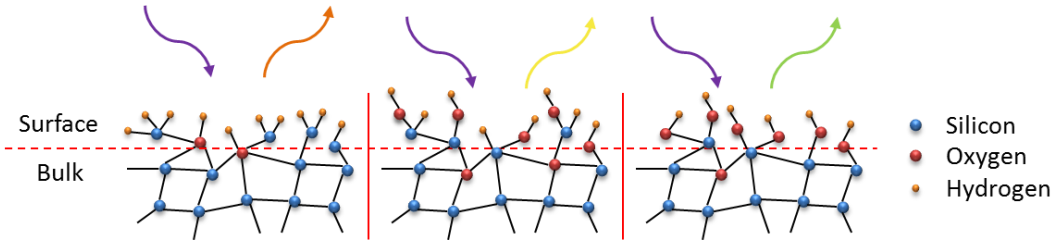

Figure 5.23 Schematic illustrations of surface species on ap-Si with concentrations of H_2O_2 increasing from left to right

Figure 5.24 presents the absorbance spectra corresponding to ap-Si containing different concentrations of H_2O_2. The orange/yellow colors that the H_2O_2:ap-Si suspensions exhibit can be seen in the spectra by a tail extending from 400 nm. As the concentration of H_2O_2 is increased, this yellow color becomes more white and the tail in the spectra also decreases. The ap-Si sample containing no H_2O_2 displayed absorbance features similar to those observed in previous samples. With the addition of more peroxide, the solution showed a dramatic change in its spectral features. The wavelength at which the suspensions absorbed a majority of the incoming light is blue shifted with increasing peroxide concentrations. This indicates a change in the electronic structure which allows for the shift in emission.

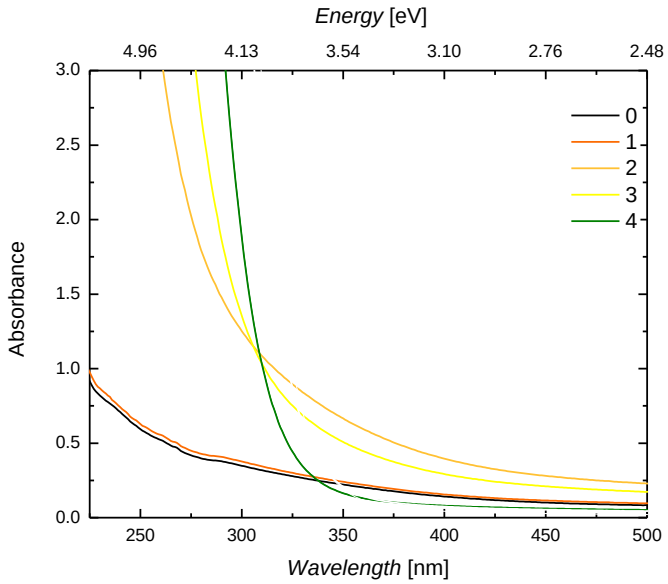

Figure 5.24 UV-Vis absorbance spectra of ap-Si with increasing H_2O_2 concentrations

5.7 Summary

In conclusion, we have successfully synthesized ap-Si suspensions through a stain etching method. Etching Si surfaces with a solution containing HF, $FeCl_3$, and HCl produced highly photoluminescent films composed of a dual layer structure. Sonicating these films removed the top layer of nodules, which were further milled through additional sonication steps. Although these particles vary greatly in size, their fluorescent properties were uniform and dependent mainly on surface properties. However, oxygen sensitivity is a major factor to overcome for both proper characterization and application. To the best of our knowledge, there has been no report of tunable emission of ap-Si found in the literature. It is also one of the few materials in which PL emission is not controlled by the size of the particles. Its unique properties make it an attractive material for a number of possible

applications. However, more work would need to be conducted to determine its electronic properties before it may be properly implemented in devices.

6 CONCLUSION

6.1 Concluding Remarks

Through the course of this work, much has been discovered about the materials created from sonicating stain etched layers of p-Si. Using an etchant mixture containing HNO_3, we created p-Si films similar to what is claimed in the literature. After sonication, colloidal suspensions were made which contained nanocrystalline particles. Although its yield was low, they exhibited interesting properties such as blue PL emission when excited by UV light, a crystal lattice that contained a different d-spacing than that found in bulk Si, and an enhancement of PL emission after reconstitution.

Stain etching with an etchant containing $FeCl_3$ and HCl yielded thick p-Si films which contained ap-Si particles. The etching pattern observed for our films were quite unique and has never been reported in the literature to our knowledge. Also, we did not find the amorphous structure reported by groups studying similar etching compositions. The ultra-bright PL emission seen in and measured for suspensions of ap-Si renders it an interesting material to study. Oxidation effects on the PL emission were shown by FT-IR measurements. Changing the surface species altered the emission and allowed it to range between red to green wavelengths. Its high degree of porosity and consequently large surface area allowed the chemical species found on the surface to have a profound effect on optical properties.

6.2 Recommendations for Future Work

Although interesting properties have been observed through this research, much more work needs to be conducted in order to fully understand and use the materials which were synthesized. For nc-Si particles, synthesis of greater concentrations of the material are necessary in order to fully characterize them. Once these quantities can be produced, analysis of the crystal structure and chemical composition should be simpler. Definitive identification of the composition and crystalline phase of nc-Si are necessary before further work on this material can be undertaken. Discovering the cause of the fluorescence enchantment which occurs after reconstituting the solutions would also be of interest.

As for ap-Si suspensions, more work could be conducted on several aspects of the synthesis, characterization, functionalization, and application of this material. Optimizing the synthesis conditions would be necessary in order to efficiently produce these suspensions for further analysis and use in devices or other applications. Listed below are our recommendations for future work on ap-Si:

- Optimizing the synthesis parameters such as etching time, etchant concentrations, type of Si substrate, etc.… would be important for producing higher yields of a consistent product.
- Along with optimizing the process, determining a method to further reduce the size of the ap-Si particles and create a uniform size distribution would be of interest for applications requiring such properties. Ball milling may be one method to achieve this.

- Understanding how the diffusions of the etching species controls the morphology of the Si surface can help explain the formation of the nodules and may help in creating thicker ap-Si films.
- Determining the mechanism responsible for the transition between crystalline to amorphous phases will aid in our understanding of the structures responsible for the observed properties in ap-Si
- Stabilizing the PL emission of ap-Si suspensions is essential for its use in opto-electronic devices. One method to prevent oxidation and tune the emission is to functionalize the surface with molecules that can both stabilize the suspensions as well as create a barrier for oxygen diffusion.
- Creating a model of the PL emission mechanism in ap-Si would help in understanding the precise cause of the emission, as well as determining the range of wavelengths which can be achieved.
- Determining the quantum yield and lifetimes of PL emission in ap-Si suspension would be important for understanding the full range of properties this material possess.

Finally, using this material in appropriate applications would be the ultimate objective. Several possible uses which ap-Si suspensions may work well in include the active material in solar cells, LEDs, Lasers, Li ion battery anodes, drug delivery systems, and catalysts.

7 REFERENCES

[1] D. R. Lide, *CRC Handbook of Chemistry and Physics*, 85th ed., vol. 16, no. 1. CRC Press, 2004, p. 2712.

[2] L. Canham, "Gaining light from silicon.," *Nature*, vol. 408, no. 6811, pp. 411-2, Nov. 2000.

[3] A. M. Rossi and H. G. Bohn, "Photodetectors from Porous Silicon," *Physica Status Solidi (a)*, vol. 202, no. 8, pp. 1644-1647, Jun. 2005.

[4] F. Ramiro-Manzano, R. Fenollosa, E. Xifré-Pérez, M. Garín, and F. Meseguer, "Porous silicon microcavities based photonic barcodes.," *Advanced Materials*, vol. 23, no. 27, pp. 3022-5, Jul. 2011.

[5] S. B.-T. de-Leon, R. Oren, M. E. Spira, N. Korbakov, S. Yitzchaik, and a. Sa'ar, "Porous silicon substrates for neurons culturing and bio-photonic sensing," *Physica Status Solidi (a)*, vol. 202, no. 8, pp. 1456-1461, Jun. 2005.

[6] J. Salonen, J. Paski, K. Vähä-Heikkilä, T. Heikkilä, M. Björkqvist, and V.-P. Lehto, "Determination of drug load in porous silicon microparticles by calorimetry," *Physica Status Solidi (a)*, vol. 202, no. 8, pp. 1629-1633, Jun. 2005.

[7] J. L. Coffer et al., "Porous silicon-based scaffolds for tissue engineering and other biomedical applications," *Physica Status Solidi (a)*, vol. 202, no. 8, pp. 1451-1455, Jun. 2005.

[8] S. Litvinenko et al., "Hydrogen production from nano-porous Si powder formed by stain etching," *International Journal of Hydrogen Energy*, vol. 35, no. 13, pp. 6773-6778, Jul. 2010.

[9] D. Dimova-Malinovska, "Application of Stain Etched Porous Silicon in Solar Cells and Light Emitting Diodes," *Functional Properties of Nanostructured Materials*, pp. 323–332, 2006.

[10] H.-C. Shin, J. a. Corno, J. L. Gole, and M. Liu, "Porous silicon negative electrodes for rechargeable lithium batteries," *Journal of Power Sources*, vol. 139, no. 1-2, pp. 314-320, Jan. 2005.

[11] A. M. Derfus, W. C. W. Chan, and S. N. Bhatia, "Probing the Cytotoxicity of Semiconductor Quantum Dots," *Nano Letters*, vol. 4, no. 1, pp. 11-18, Jan. 2004.

[12] E. J. Henderson et al., "Colloidally Stable Silicon Nanocrystals with Near-Infrared Photoluminescence for Biological Fluorescence Imaging.," *Small*, no. 17, pp. 2507-2516, Jul. 2011.

[13] Y. Choi, G. Wang, M. H. Nayfeh, and S.-T. Yau, "A hybrid biofuel cell based on electrooxidation of glucose using ultra-small silicon nanoparticles.," *Biosensors & bioelectronics*, vol. 24, no. 10, pp. 3103-7, Jun. 2009.

[14] D. P. Puzzo, E. J. Henderson, M. G. Helander, Z. Wang, G. a Ozin, and Z. Lu, "Visible colloidal nanocrystal silicon light-emitting diode.," *Nano letters*, vol. 11, no. 4, pp. 1585-90, Apr. 2011.

[15] C.-Y. Liu, Z. C. Holman, and U. R. Kortshagen, "Hybrid solar cells from P3HT and silicon nanocrystals.," *Nano letters*, vol. 9, no. 1, pp. 449-52, Jan. 2009.

[16] Q. Liu, M. H. Nayfeh, and S.-T. Yau, "Supercapacitor electrodes based on polyaniline–silicon nanoparticle composite," *Journal of Power Sources*, vol. 195, no. 12, pp. 3956-3959, Jun. 2010.

[17] G. Wang, S. Yau, K. Mantey, and M. Nayfeh, "Fluorescent Si nanoparticle-based electrode for sensing biomedical substances," *Optics Communications*, vol. 281, no. 7, pp. 1765-1770, Apr. 2008.

[18] M. H. Nayfeh et al., "Observation of laser oscillation in aggregates of ultrasmall silicon nanoparticles," *Applied Physics Letters*, vol. 80, no. 1, p. 121, 2002.

[19] A. Li and B. Draine, "Are silicon nanoparticles an interstellar dust component?," *The Astrophysical Journal*, vol. 564, no. 2002, p. 803, 2002.

[20] L. T. Canham, "Silicon quantum wire array fabrication by electrochemical and chemical dissolution of wafers," *Applied Physics Letters*, vol. 57, no. 10, p. 1046, 1990.

[21] G. Korotcenkov and B. K. Cho, "Silicon Porosification: State of the Art," *Critical Reviews in Solid State and Materials Sciences*, vol. 35, no. 3, pp. 153-260, Aug. 2010.

[22] T. Young, C. Chen, J. Liou, Y. Yang, and T. Chang, "Study on the Si–Si Vibrational States of the Near Surface Region of Porous Silicon," *Journal of Porous Materials*, vol. 7, no. 1, pp. 339–343, 2000.

[23] A. Cullis, L. T. Canham, and P. D. J. Calcott, "The structural and luminescence properties of porous silicon," *Applied Physics Reviews*, vol. 82, no. 3, pp. 909-965, 1997.

[24] G. Belomoin et al., "Observation of a magic discrete family of ultrabright Si nanoparticles," *Applied Physics Letters*, vol. 80, no. 5, p. 841, 2002.

[25] J. G. C. Veinot, "Synthesis, surface functionalization, and properties of freestanding silicon nanocrystals.," *Chemical communications*, no. 40, pp. 4160-8, Oct. 2006.

[26] A. Cullis and L. Canham, "Visible light emission due to quantum size effects in highly porous crystalline silicon," *Nature*, vol. 353, pp. 335-338, 1991.

[27] M. H. Nayfeh and L. Mitas, "Silicon Nanoparticles: New Photonic and Electronic Material at the Transition Between Solid and Molecule," in *Nanosilicon*, 2007, pp. 3-75.

[28] D. Nielsen, L. Abuhassan, M. Alchihabi, a. Al-Muhanna, J. Host, and M. H. Nayfeh, "Current-less anodization of intrinsic silicon powder grains: Formation of fluorescent Si nanoparticles," *Journal of Applied Physics*, vol. 101, no. 11, p. 114302, 2007.

[29] K. W. Kolasinski, "Silicon nanostructures from electroless electrochemical etching," *Current Opinion in Solid State and Materials Science*, vol. 9, no. 1-2, pp. 73-83, Feb. 2005.

[30] K. W. Kolasinski, "Charge Transfer and Nanostructure Formation During Electroless Etching of Silicon," *The Journal of Physical Chemistry C*, no. 2, p. 2834, 2010.

[31] R. Fathauer, T. George, A. Ksendzov, and R. Vasquez, "Visible luminescence from silicon wafers subjected to stain etches," *Applied Physics Letters*, vol. 60, no. 8, pp. 995–997, 1992.

[32] M. Nahidi and K. W. Kolasinski, "Effects of Stain Etchant Composition on the Photoluminescence and Morphology of Porous Silicon," *Journal of The Electrochemical Society*, vol. 153, no. 1, p. C19, 2006.

[33] X. Li, Y. He, S. S. Talukdar, and M. T. Swihart, "Process for Preparing Macroscopic Quantities of Brightly Photoluminescent Silicon Nanoparticles with Emission Spanning the Visible Spectrum," *Langmuir*, vol. 19, no. 20, pp. 8490-8496, Sep. 2003.

[34] B. A. Manhat et al., "One-Step Melt Synthesis of Water-Soluble, Photoluminescent, Surface-Oxidized Silicon Nanoparticles for Cellular Imaging Applications," *Chemistry of Materials*, vol. 23, no. 9, pp. 2407-2418, May 2011.

[35] D. Mayeri, B. L. Phillips, M. P. Augustine, and S. M. Kauzlarich, "NMR Study of the Synthesis of Alkyl-Terminated Silicon Nanoparticles from the Reaction of SiCl 4 with the Zintl Salt , NaSi," *Symposium A Quarterly Journal In Modern Foreign Literatures*, vol. 727, no. 14, pp. 765-770, 2001.

[36] J. Zou, P. Sanelle, K. a. Pettigrew, and S. M. Kauzlarich, "Size and Spectroscopy of Silicon Nanoparticles Prepared via Reduction of SiCl4," *Journal of Cluster Science*, vol. 17, no. 4, pp. 565-578, Nov. 2006.

[37] T. Seto et al., "Synthesis of size-selected silicon nanoparticles by laser ablation," *Journal of Aerosol Science*, vol. 31, no. 1, pp. 628–629, 2000.

[38] R. a. Bley, S. M. Kauzlarich, J. E. Davis, and H. W. H. Lee, "Characterization of Silicon Nanoparticles Prepared from Porous Silicon," *Chemistry of Materials*, vol. 8, no. 8, pp. 1881-1888, Jan. 1996.

[39] a Troia, a Giovannozzi, and G. Amato, "Preparation of tunable silicon q-dots through ultrasound.," *Ultrasonics sonochemistry*, vol. 16, no. 4, pp. 448-51, Apr. 2009.

[40] A. a Bagabas, M. a Gondal, M. a Dastageer, A. a Al-Muhanna, T. H. Alanazi, and M. a Ababtain, "A study of laser-induced blue emission with nanosecond decay of silicon nanoparticles synthesized by a chemical etching method.," *Nanotechnology*, vol. 20, no. 35, p. 355703, Sep. 2009.

[41] R. Street, "Luminescence and recombination in hydrogenated amorphous silicon," *Advances in physics*, vol. 30, no. 5, pp. 593-676, 1981.

[42] N.-M. Park, T.-S. Kim, and S.-J. Park, "Band gap engineering of amorphous silicon quantum dots for light-emitting diodes," *Applied Physics Letters*, vol. 78, no. 17, p. 2575, 2001.

[43] R. Anthony and U. Kortshagen, "Photoluminescence quantum yields of amorphous and crystalline silicon nanoparticles," *Physical Review B*, vol. 80, no. 11, pp. 1-6, Sep. 2009.

[44] I. Solomon, R. . Wehrspohn, J.-N. Chazalviel, and F. Ozanam, "Spatial and quantum confinement in crystalline and amorphous porous silicon," *Journal of Non-Crystalline Solids*, vol. 227-230, pp. 248-253, May 1998.

[45] M. J. Estes, L. R. Hirsch, S. Wichart, G. Moddel, and D. L. Williamson, "Visible photoluminescence from porous a-Si:H and porous a-Si:C:H thin films," *Journal of Applied Physics*, vol. 82, no. 4, p. 1832, 1997.

[46] N. Ovsyuk and V. Novikov, “Influence of structural disorder on Raman scattering in amorphous porous silicon,” *Physical Review B*, vol. 57, no. 23, pp. 615-618, 1998.

[47] C. Meier, A. Gondorf, S. Lüttjohann, A. Lorke, and H. Wiggers, “Silicon nanoparticles: Absorption, emission, and the nature of the electronic bandgap,” *Journal of Applied Physics*, vol. 101, no. 10, p. 103112, 2007.

[48] R. K. Soni, L. F. Fonseca, O. Resto, M. Buzaianu, and S. Z. Weisz, “Size-dependent optical properties of silicon nanocrystals,” *Journal of Luminescence*, vol. 83-84, pp. 187-191, Nov. 1999.

[49] N. Shirahata, T. Tsuruoka, T. Hasegawa, and Y. Sakka, “Size-tunable UV-luminescent silicon nanocrystals.,” *Small*, vol. 6, no. 8, pp. 915-21, Apr. 2010.

[50] E. J. Henderson, J. a. Kelly, and J. G. C. Veinot, “Influence of HSiO 1.5 Sol–Gel Polymer Structure and Composition on the Size and Luminescent Properties of Silicon Nanocrystals,” *Chemistry of Materials*, vol. 21, no. 22, pp. 5426-5434, Nov. 2009.

[51] W. L. Wilson, P. F. Szajowski, and L. E. Brus, “Quantum confinement in size-selected, surface-oxidized silicon nanocrystals.,” *Science*, vol. 262, no. 5137, pp. 1242-4, Nov. 1993.

[52] F. Koch and V. Petrova-Koch, “Light from Si-nanoparticle systems - a comprehensive view,” *Journal of non-crystalline Solids*, vol. 198, pp. 840–846, 1996.

[53] M. Wolkin, J. Jorne, P. Fauchet, G. Allan, and C. Delerue, “Electronic States and Luminescence in Porous Silicon Quantum Dots: The Role of Oxygen,” *Physical Review Letters*, vol. 82, no. 1, pp. 197-200, Jan. 1999.

[54] M. K. Lee and K. R. Peng, “Blue emission in porous silicon,” *Applied Physics Letters*, vol. 62, no. 24, pp. 3159-3160, Mar. 1993.

[55] H. Tamura, M. Ruckschloss, T. Wirschem, and S. Veprek, “Origin of the green/blue luminescence from nanocrystalline silicon,” *Applied physics letters*, vol. 65, no. 12, pp. 1537–1539, 1994.

[56] N. Shirahata, D. Hirakawa, and Y. Sakka, “Interfacial-related color tuning of colloidal Si nanocrystals,” *Green Chemistry*, vol. 12, no. 12, p. 2139, 2010.

[57] N. Shirahata, “Colloidal Si nanocrystals: a controlled organic-inorganic interface and its implications of color-tuning and chemical design toward

sophisticated architectures.," *Physical chemistry chemical physics : PCCP*, vol. 13, no. 16, pp. 7284-94, Apr. 2011.

[58] Y. Kanemitsu, "Light-emitting silicon materials," *Journal of luminescence*, vol. 70, no. 1, pp. 333–342, 1996.

[59] P. Deák, M. Rosenbauer, M. Stutzmann, J. Weber, and M. Brandt, "Siloxene: Chemical quantum confinement due to oxygen in a silicon matrix," *Physical Review Letters*, vol. 69, no. 17, pp. 2531-2534, Oct. 1992.

[60] H. Fuchs, M. Stutzmann, M. Brandt, M. Rosenbauer, J. Weber, and M. Cardona, "Visible luminescence from porous silicon and siloxene," *Physica Scripta*, vol. 45, pp. 309-313, 1992.

[61] P. McCord, S. L. Yau, and A. J. Bard, "Chemiluminescence of anodized and etched silicon: Evidence for a luminescent siloxene-like layer on porous silicon," *Science*, vol. 257, no. 5066, p. 68, 1992.

[62] S. O. Kasap, "Amorphous Semiconductors," in *Principles of Electronic Materials and Devices*, 3rd ed., New York: McGraw-Hill Book Co., 2006, pp. 458-451.

[63] J. M. Perez et al., "Direct evidence for the amorphous silicon phase in visible photoluminescent porous silicon," *Applied Physics Letters*, vol. 61, no. 5, p. 563, 1992.

[64] E. Bustarret, M. Ligeon, and L. Ortega, "Visible light emission at room temperature from partially oxidized amorphous silicon," *Solid state communications*, vol. 83, no. 7, pp. 461–464, 1992.

[65] R. Wehrspohn, J. Chazalviel, F. Ozanam, and I. Solomon, "Conditions of Elaboration of Luminescent Porous Silicon from Hydrogenated Amorphous Silicon.," *Physical review letters*, vol. 77, no. 9, pp. 1885-1888, Aug. 1996.

[66] M. Estes and G. Moddel, "Luminescence from amorphous silicon nanostructures.," *Physical review. B, Condensed matter*, vol. 54, no. 20, pp. 14633-14642, Nov. 1996.

[67] M. J. Estes and G. Moddel, "A model of size-dependent photoluminescence in amorphous silicon nanostructures: Comparison with observations of porous silicon," *Applied Physics Letters*, vol. 68, no. 13, p. 1814, 1996.

[68] R. B. Wehrspohn, J.-N. Chazalviel, F. Ozanam, and I. Solomon, "Spatial versus quantum confinement in porous amorphous silicon nanostructures," *The European Physical Journal B*, vol. 8, no. 2, pp. 179-193, Mar. 1999.

[69] M. T. Kelly, J. K. M. Chun, and A. B. Bocarsly, "High efficiency chemical etchant for the formation of luminescent porous silicon," *Applied Physics Letters*, vol. 64, no. 13, p. 1693, 1994.

[70] M. E. Dudley and K. W. Kolasinski, "Structure and photoluminescence studies of porous silicon formed in ferric ion containing stain etchants," *Physica Status Solidi (a)*, vol. 206, no. 6, pp. 1240-1244, Jun. 2009.

[71] M. E. Dudley and K. W. Kolasinski, "Stain Etching with Fe(III), V(V), and Ce(IV) to Form Microporous Silicon," *Electrochemical and Solid-State Letters*, vol. 12, no. 4, p. D22, 2009.

[72] D. Brandon and W. D. Kaplan, *Microstructural Characterization of Materials*, 2nd ed. John Wiley & Sons, 2008, p. 550.

[73] F. Rouquérol, J. Rouquerol, and K. Sing, *Adsorption by Powders & Porous Solids: Principles, Methodology and Applications*. Academic Press, 1999, p. 467.

[74] J. R. Ferrero, K. Nakamoto, and C. W. Brown, *Introductory Raman Spectroscopy*, 2nd ed. Academic Press, 2003, p. 434.

[75] J. Coates, "Interpretation of Infrared Spectra, A Practical Approach," in *Encyclopedia of Analytical Chemistry*, R. A. Mayers, Ed. John Wiley & Sons Ltd., 2000, pp. 10815-10837.

[76] D. Dragoman and M. Dragoman, *Optical Characterization of Solids*, 1st ed. Springer, 2002, p. 451.

[77] L. Schirone, "On the morphology of stain-etched porous silicon films," *Journal of Luminescence*, vol. 80, no. 1-4, pp. 163-167, Dec. 1998.

[78] R. R. Kunz, P. M. Nitishin, H. R. Clark, M. Rothschild, and B. Ahern, "Observation of a nanocrystalline-to-amorphous phase transition in luminescent porous silicon," *Applied Physics Letters*, vol. 67, no. 12, p. 1766, 1995.

[79] E. A. Travnicek and J. H. Weber, "Continous Dissolution of Copper by Nitric Acid," *Journal of Physical Chemistry*, vol. 65, no. 2, pp. 235-240, Feb. 1961.

[80] Y. Zhang, Z. Iqbal, S. Vijayalakshmi, and H. Grebel, "Stable hexagonal-wurtzite silicon phase by laser ablation," *Applied Physics Letters*, vol. 75, no. 18, p. 2758, 1999.

[81] M. Hosaka and S. Taki, "Hydrothermal growth of quartz crystals in NaCl solution," *Journal of Crystal Growth*, vol. 52, no. 25, pp. 837-842, Apr. 1981.

[82] C.-S. Yang, R. a. Bley, S. M. Kauzlarich, H. W. H. Lee, and G. R. Delgado, "Synthesis of Alkyl-Terminated Silicon Nanoclusters by a Solution Route," *Journal of the American Chemical Society*, vol. 121, no. 22, pp. 5191-5195, Jun. 1999.

[83] W. J. Salcedo, F. Ramirez Fernandez, and E. Galeazzo, "Structural characterization of photoluminescent porous silicon with FTIR spectroscopy," *Brazilian Journal of Physics*, vol. 27, no. 4, pp. 158–161, 1997.

[84] M. Ray et al., "Blue–violet photoluminescence from colloidal suspension of nanocrystalline silicon in silicon oxide matrix," *Solid State Communications*, vol. 149, no. 9-10, pp. 352-356, Mar. 2009.

[85] S. Wang, C. Querner, T. Dadosh, C. H. Crouch, D. S. Novikov, and M. Drndic, "Collective fluorescence enhancement in nanoparticle clusters.," *Nature communications*, vol. 2, p. 364, Jan. 2011.

[86] T. George, R. Vasquez, S. Kim, R. W. Fathauer, and W. Pike, "Porous Amorphous Si Formation by the Etching of Single Crystal Si Substrates," in *MRS Proceedings*, 1992, vol. 259, no. 1, pp. 415-420.

[87] S. K. Deb, M. Wilding, M. Somayazulu, and P. F. Mcmillan, "Pressure-induced amorphization and amorphous-amorphous transistion in densified porous silicon," *Nature*, vol. 414, no. November, pp. 18-20, 2001.

[88] M. C. Rossi, S. Salvatori, F. Galluzzi, and G. Conte, "Laser-induced nanocrystalline silicon formation in a-SiO matrices," *Materials Science and Engineering: B*, vol. 69-70, pp. 299-302, Jan. 2000.

[89] S. Goodes, T. Jenkins, M. Beale, and C. Pickering, "The characterisation of porous silicon by Raman spectroscopy," *Semiconductor Science and Technology*, vol. 3, p. 483, 1988.

[90] M. Brodsky, M. Cardona, and J. Cuomo, "Infrared and Raman spectra of the silicon-hydrogen bonds in amorphous silicon prepared by glow discharge and sputtering," *Physical Review B*, vol. 16, no. 8, pp. 3556-3571, Oct. 1977.

[91] D. Beeman, R. Tsu, and M. Thorpe, "Structural information from the Raman spectrum of amorphous silicon," *Physical Review B*, vol. 32, no. 2, pp. 874-878, 1985.

[92] M. Ivanda, K. Furić, and O. Gamulin, "'Boson' peak in Raman spectra of hydrogenated amorphous silicon," *Journal of Non Crystalline Solids*, vol. 138, pp. 103-106, 1991.

[93] R. P. Vasquez, R. W. Fathauer, T. George, A. Ksendzov, and T. L. Lin, "Electronic structure of light-emitting porous Si," *Applied Physics Letters*, vol. 60, no. 8, p. 1004, 1992.

[94] K. Littau, P. Szajowski, A. Muller, A. Kortan, and L. Brus, "A luminescent silicon nanocrystal colloid via a high-temperature aerosol reaction," *The Journal of Physical Chemistry*, vol. 97, no. 6, pp. 1224–1230, 1993.

[95] M. G. Bawendi, P. J. Carroll, W. L. Wilson, and L. E. Brus, "Luminescence properties of CdSe quantum crystallites: Resonance between interior and surface localized states," *The Journal of Chemical Physics*, vol. 96, no. 2, p. 946, 1992.

[96] T. Muschik, R. Schwarz, and F. Karg, "Characterization of band tail states in amorphous silicon alloys by temperature dependent photoluminescence," *Journal of Luminescence*, vol. 48-49, pp. 636-640, Jan. 1991.

[97] M. Cardona, "Vibrational Spectra of Hydrogen in Silicon and Germanium," *physica status solidi (b)*, vol. 118, no. 2, pp. 463-481, Aug. 1983.

[98] D. B. Mawhinney, J. A. Glass Jr, and J. T. Yates Jr, "FTIR study of the oxidation of porous silicon," *The Journal of Physical Chemistry B*, vol. 101, no. 7, pp. 1202–1206, 1997.

[99] Y. Ishikawa, "Low-Temperature Oxidation of Silicon in H 2 O 2 Ambient by UV Irradiation," *Japanese Journal of Applied Physics*, vol. 41, no. Part 1, No. 3A, pp. 1324-1325, Mar. 2002.

8 APPENDICES

8.1 IR Absorbance

- Typically employed to measures bond vibration frequencies in molecules and is used to determine **functional groups**
- Summary: http://www.phys.ubbcluj.ro/~dana.maniu/OS/BS_2.pdf
- Is also used to study bulk and surface properties of inorganic materials
- Molecules absorb specific frequencies that are characteristic of their structure
- For a vibrational mode in a molecule to be IR active, it must be associated with changes in the dipole moment (**polar bonds**) (to allow for interaction with the alternating electrical component of the IR radiation wave
- IR range is between 4000-400 cm^{-1}, wavenumbers (reciprocal of the wavelength) are proportional to frequency/energy
- Vibrational frequencies for **stretching** bonds in molecules are related to the strength of the chemical bonds and the masses of the atoms
- Coupling between the stretching and bending vibrations may occur if the stretching bond form one side of the angle that varies in the bending vibration of the same symmetry species
- Simple stretching is found between 3500-1600 cm^{-1}
- Complex vibrations: 1400-400 cm^{-1}
- Non-linear molecules with N atoms: 2N-6 normal modes: N-1 stretching and 2N-5 bending
- Visualizations of vibrational modes:
- http://www.d.umn.edu/~pkiprof/ChemWebV2/Vibrations/vib3.html
- http://www.d.umn.edu/~pkiprof/ChemWebV2/Vibrations/vib2.html
- Fundamental vibrational frequency, ν, of a molecular ensemble can be express by a Hooke's law
  - $\boldsymbol{\nu = \frac{1}{2\pi c}\sqrt{\frac{\kappa}{\mu}}}$
- Where μ is the reduced mass given by $m_1m_2/(m_1+m_2)$ with m_1 and m_2 being component masses of the chemical bonds, and κ is the force constant.
- Calculations of vibrations modes for Si-H_x can be found in ref. [97]

8.2 Sonication Effects on Toluene

After sonication using the probe sonicator was found that in addition to fluorescent ap-Si, there was a contribution to the PL spectra of the suspensions coming from toluene. **Figure 8.1** shows the PL emission spectra of pure toluene, before and after sonicating for 30 minutes. It can be seen that before sonication the solution does not emit any considerable PL emission. After sonication an emission peak at 430 nm forms, and is intense enough to be observed with the naked eye.

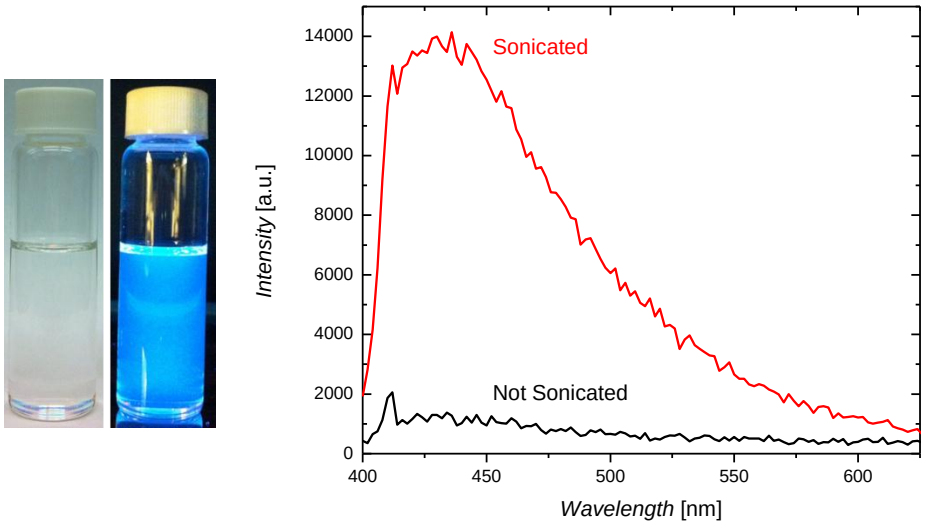

Figure 8.1 Left: image of toluene after sonication, under white light and under 365 nm UV illumination. Right: PL emission spectra of toluene before(black) and after(red) sonication at 365 nm excitation

FT-IR absorbance measurements were taken of the toluene solutions before and after sonication to see if the formation of a new functional group can be identified as the source of this emission. As presented in **Figure 8.2**, it was found that the toluene showed all the characteristic peaks of the solvent both before and after sonication. Samples were then dried to see if a new compound may have formed which was not visible in the wet measurements. The dried samples also showed the same IR spectra before and after the sonication treatment. The peaks displayed correspond to C-H bonding, which is most likely due to residual solvent on the pressed NaCl pellets.

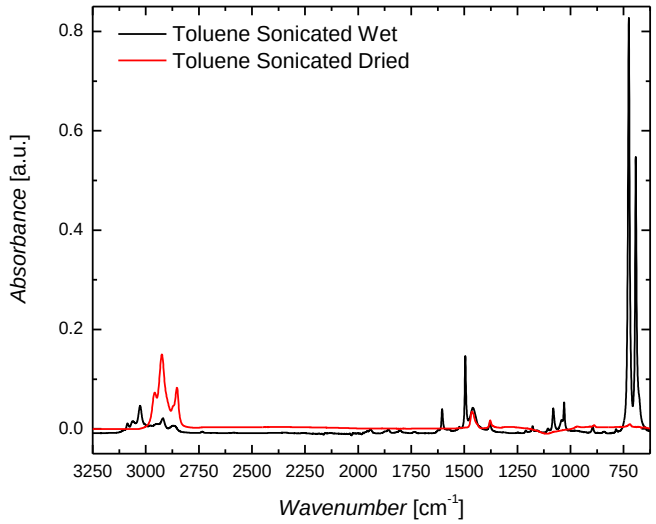

Figure 8.2 FT-IR absorbance spectra of toluene wet (black) and dried into NaCl pellet (red)